NASA CONTRACTOR
REPORT

NASA CR-144246

(NASA-CR-144246) GATE-CONTROLLED-DIODES IN SILICON-ON-SAPPHIRE: A COMPUTER SIMULATION Interim Report (Mississippi State Univ., Mississippi State.) 83 p HC $5.00 CSCL 09C

N76-22459

G3/33

Unclas
26767

GATE-CONTROLLED-DIODES IN SILICON-ON-SAPPHIRE A COMPUTER SIMULATION

By J. D. Gassaway

Mississippi State University
Department of Electrical Engineering
Mississippi State, Mississippi 39762

September 8, 1974

Interim Report

Prepared for

NASA-GEORGE C. MARSHALL SPACE FLIGHT CENTER
Marshall Space Flight Center, Alabama 35812

TECHNICAL REPORT STANDARD TITLE PAGE

1. REPORT NO. CR-144246	2. GOVERNMENT ACCESSION NO.	3. RECIPIENT'S CATALOG NO.
4. TITLE AND SUBTITLE GATE-CONTROLLED-DIODES IN SILICON-ON-SAPPHIRE A Computer Simulation		5. REPORT DATE February 10, 1976
		6. PERFORMING ORGANIZATION CODE
7. AUTHOR(S) J. D. Gassaway		8. PERFORMING ORGANIZATION REPORT # EIRS-EE-75-1
9. PERFORMING ORGANIZATION NAME AND ADDRESS Mississippi State University Department of Electrical Engineering Mississippi State, Mississippi 39762		10. WORK UNIT NO.
		11. CONTRACT OR GRANT NO. NAS8-26749
		13. TYPE OF REPORT & PERIOD COVERED Contractor Report September 8, 1974
12. SPONSORING AGENCY NAME AND ADDRESS National Aeronautics and Space Administration George C. Marshall Space Flight Center Marshall Space Flight Center, Alabama 35812		14. SPONSORING AGENCY CODE EC45
15. SUPPLEMENTARY NOTES Electronics Development Division, Electronics and Control Laboratory Design Techniques Branch		

16. ABSTRACT

This report deals with computer simulation of the electrical behavior of a Gate-Controlled Diode (GCD) fabricated in Silicon-On-Sapphire (SOS). In particular it was of interest to establish a procedure for determining life-time profiles from capacitance and reverse current measurements on the GCD. Chapter 1 discusses the SOS structure and points out the need of lifetime profiles to assist in device design for CCD's and bipolar transistors. Chapter 2 presents the one-dimensional analytical formula for electrostatic analysis of the SOS-GCD which are useful for data interpretation and setting boundary conditions on a simplified two-dimensional analysis. Chapter 3 gives the results of a two-dimensional analysis which treats the field as one-dimensional until the silicon film is depleted and the field penetrates the sapphire substrate. Chapter 4 describes a more complete two-dimensional model and gives results of programs implementing the model.

17. KEY WORDS	18. DISTRIBUTION STATEMENT Unclassified-Unlimited COR: John M. Gould EC01 F. Brooks Moore Director, E&C Lab

19. SECURITY CLASSIF. (of this report)	20. SECURITY CLASSIF. (of this page)	21. NO. OF PAGES	22. PRICE
Unclassified	Unclassified	80	NTIS

MSFC - Form 3292 (Rev December 1972)

For sale by National Technical Information Service, Springfield, Virginia 22151

ACKNOWLEDGEMENTS

It is a pleasure to acknowledge the contributions of Dr. Ditmar Kranzer to this work. Dr. Kranzer provided the author with extensive experimental data on the SOS-GCD which he had obtained and has not published at this time. In conversations he contributed suggestions concerning the modeling procedure and also provided information concerning the experimental techniques and equipment which he used. All of these contributions were most helpful.

Some of the calculations were run on the Sigma V machine in the Electronic Components Division at MSFC. Mr. Bill Feltner was most helpful in providing assistance concerning the use of the disc memory which was essential for some of the work.

TABLE OF CONTENTS

LIST OF FIGURES

CHAPTER 1

INTRODUCTION

There has been a continuing interest in the use of silicon-on-sapphire, SOS, as a material for fabrication of high frequency electronic devices. The SOS technology allows dielectric isolation of devices by etching out isolated islands of silicon film on the high resistivity sapphire substrate in which individual devices are constructed by diffusion, oxidation, metallization, etc., implemented using photolithographic definition techniques. Because of the low lifetime in thin silicon films on sapphire, practical bipolar transistors have not been realized using this technology; however, MOS circuitry is now manufactured in SOS (Inselek, RCA, and perhaps others.) It seems likely that CCD's (Charge Coupled Devices) built in SOS may be attractive for two reasons.

First, it may at some time be desirable to integrate CCDs with other high speed SOS logic circuitry. As we shall see, CCD's will probably require thicker films, as will probably be the case for bipolar transistors, and this poses technological problems for etching. The thin film is more desirable since the etch time is reduced and the photoresist protection problem is less severe.

Perhaps a better case can be made for the desirability of fabricating CCD imaging devices in SOS. There are problems in accomplishing this, but the problems of building other CCD imagers must also be considered in comparison. The central problem in fabricating a CCD is to prevent potential barriers (or wells) between the transfer electrodes. There are three techniques which have been successful in overcoming the problem of potential barriers in the gap which result in the case of a simple structure with gaps wider than 1-2 μ m. (1) The technique used by Texas Instruments[1] makes the gap very small by depositing half of the aluminum electrodes and then anodizing them, producing an Al_2O_3 insulator, roughly 1000 Å thick, to insulate these electrodes from a subsequently deposited aluminum layer. (2) A technique proposed at Bell Labs[2] utilizes intergap doping to establish a potential within the gap to a value between those under the transmitting and receiving transfer gates. (3) Researchers at RCA[3] have published a number of papers giving results obtained with two levels of metalization, where one conductor level is doped polysilicon. Another technique which has been mentioned is the resistive sea of polysilicon in which the transfer electrode pattern is defined by doping. A short discussion of these techniques will be beneficial.

The first technique appears to be the best for solving the problem. It is simple in concept and implementation and produces, insofar as reported, no undesirable side effects such as oxide contamination for example. A high conductivity transfer electrode structure is defined in this way and the gap potential is fixed by the surface potentials under adjacent electrodes. From the standpoint of imaging, the channel is closed to incident radiation so that backside illumination is required. Therefore, the wafer must be thinned in the channel region to a thickness of roughly 30 μ m, i.e., the spacing between adjacent cells. The second technique essentially results in a self-aligned bucket-brigade structure which has a higher transfer inefficiency and consequently a lower upper cutoff frequency than a true charge coupled device. Otherwise, the structure allows wide gaps for enhancing the photon receiving area of the channel.

The third technique utilizes doped polysilicon electrodes which at best have a resistivity over ten times that of aluminum. Consequently, in long structures the resultant RC transmission structure for the polysilicon transfer electrode structure produces phase delay and distortion which limits the upper frequency of operation. The polysilicon-oxide-silicon thin film structure will result in spectral selectivity of the incident radiation, and there will of course be some absorption of radiation in the polysilicon. This latter feature of absorption will be inherent in any scheme except number two above.

Although all of these schemes may prove satisfactory in some applications, they obviously have problems associated with them. In a preceding report,[4] it was suggested that a thin film silicon-on-sapphire structure might be feasible. From an optical standpoint such a structure would be superior because the sapphire is transparent and most of the photons would be absorbed in the depletion region of the CCD channel. Kranzer[5] has reported lifetime profiles in SOS films which show that the thermal (leakage) current from depleted regions near the silicon-sapphire interface would be excessive for sensitive SOS imaging devices. His results suggest that thicker silicon films will be required for successful application of SOS to CCD imaging devices. Either of the techniques (1) or (3) above should be suitable for transfer electrode structure.

Kranzer[6] has done extensive experimentation with gate controlled diodes in which the capacitance and leakage current were measured for various conditions. Meyer[7] has also reported results from experiments with this type of structure. These results should be valuable for the design of CCD imagers and perhaps for bipolar transistors fabricated in SOS.

Figures 1.1 and 1.2 show typical results obtained by Kranzer.[6] His published data[5] was obtained using the one-dimensional Poisson's analysis to reduce both capacitance and diode reverse current vs. gate bias data to obtain lifetime and doping profiles for depletion depths short of the silicon-sapphire interface. The results of a one-dimensional analysis can be expressed as:

$$X_d = \varepsilon_{si} / C_{si} \qquad 1.1$$

$$\tau = 1/2 \; q n_i A / (\partial I_r / \partial X_d) \qquad 1.2$$

$$N_B(X_d) = - (C_T/q) \; \partial V_G / \partial X_d \qquad 1.3$$

$$C_{si} = C_T \, C_{ox} / (C_{ox} - C_T) \qquad 1.4$$

Where C_T, C_{si} and C_{ox} are respectively, the measured gate less overlap capacitance, the series depletion capacitance, and the gate to depletion layer capacitance through the oxide. Other variables are τ, the carrier lifetime, n_i the intrinsic carrier concentration, ε_{si} the silicon permittivity, V_G, the gate voltage, I_r, the diode reverse current, q, the electronic charge, A, the area of capacitance C_{si}, and X_d, the depletion layer depth.

There are certain features of Kranzer's data[6] which are not explained by a one-dimensional analysis. Furthermore, it would be of interest to have the results of a more complete analysis to study the data in the region in which the one-dimensional interpretation has reasonable validity. This study was conducted to obtain an analysis based upon an essentially two-dimensional model. The structure studied has cylindrical symmetry so that only the Z-axis and radial coordinates are required.

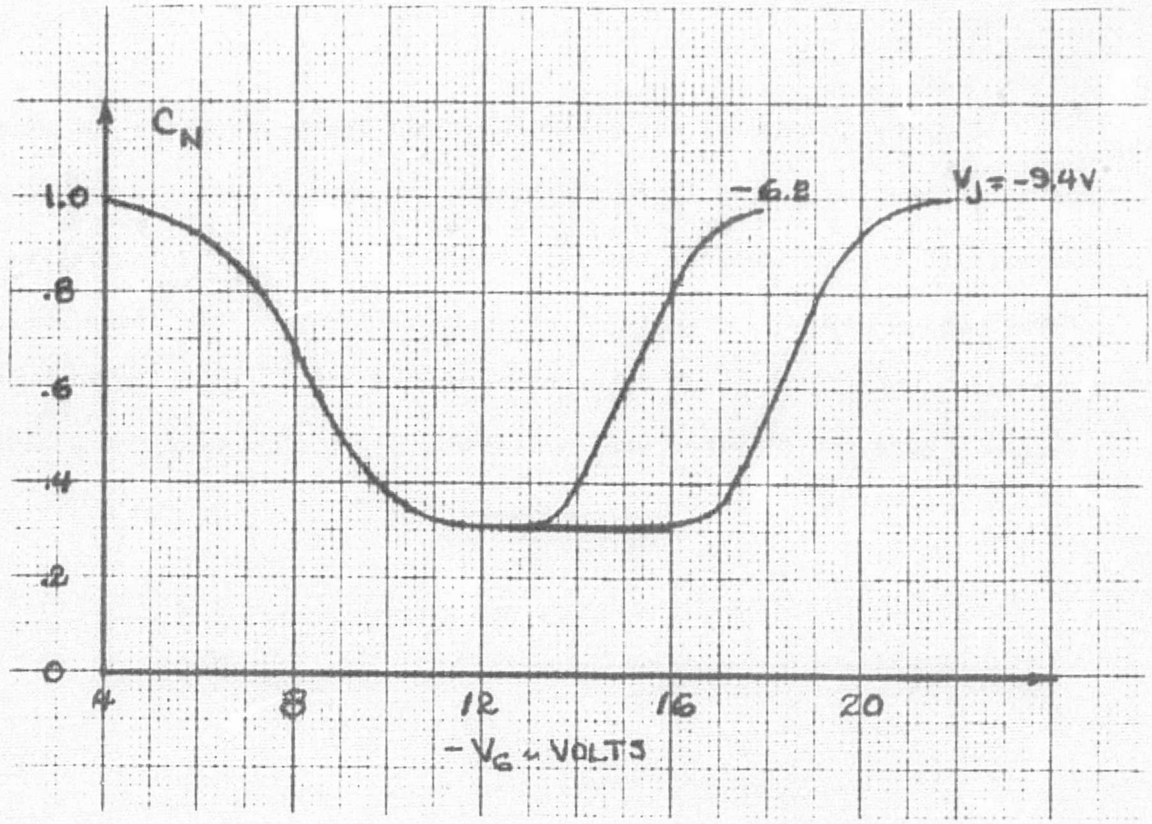

Figure 1.1 Capacitance vs. Gate Bias for SOS-GCD

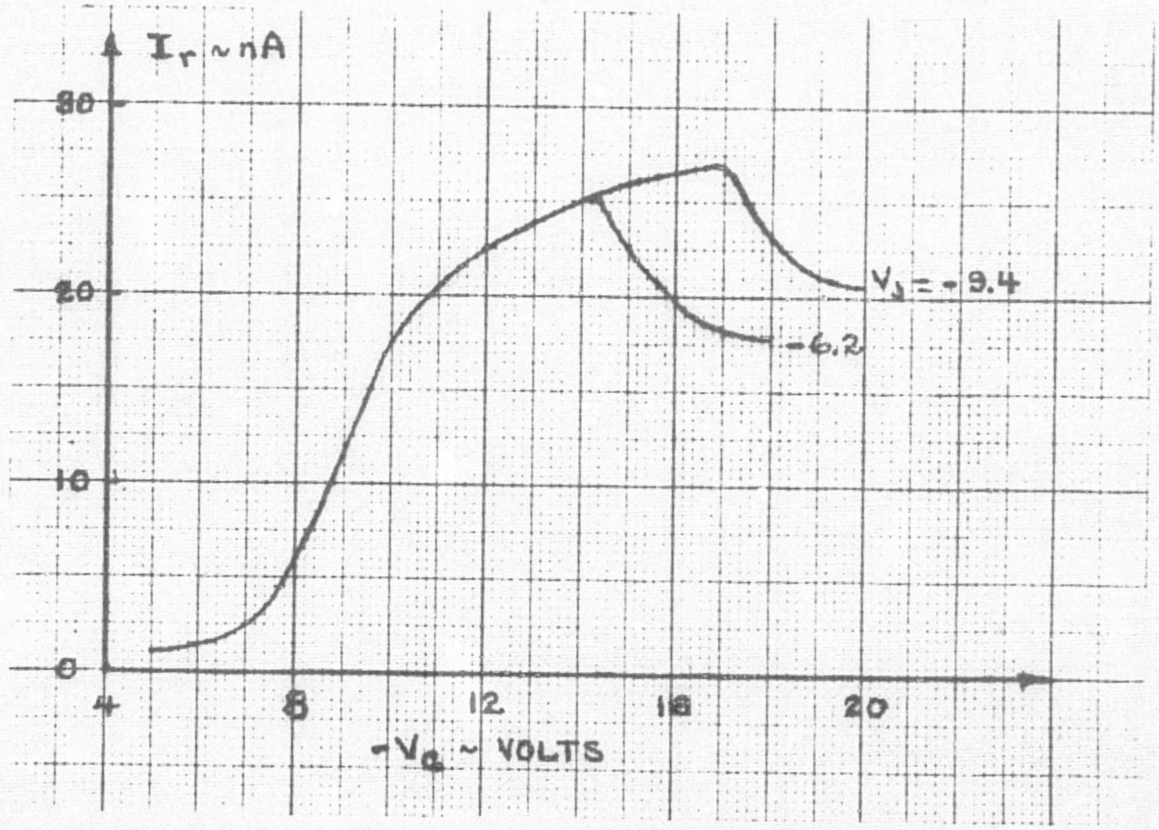

Figure 1.2 Junction Current vs. Gate Bias for SOS-GCD

Chapter 2 presents the one-dimensional analysis of the MOS structure as it is applied in the succeeding work. Chapter 3 presents a somewhat simplified two-dimensional analysis which is useful for interpreting the experimental results. Chapter 4 presents a more complete two-dimensional analysis. Chapter 5 gives the conclusions of this study. Appendices A, B, and C give the computer programs developed to implement the analysis.

CHAPTER 2

ONE-DIMENSIONAL DEPLETION

LAYER ANALYSIS OF MIS STRUCTURE

A diagram of the structure to be modeled is shown in Figure 2.1. The capacitance structure is annular with typical dimensions given in the figure where the aspect ratio of the differential radius, W_2, to the thickness is greater than 100. If the silicon-sapphire interface is accumulated with mobile carriers, thus providing a conductive plane, then clearly the silicon depletion field variation across the film thickness can be closely approximated by a one-dimensional Poisson equation solution. The presence of the P+ inner annulus and the N+ outer annulus will give rise to a small radial field component. The fact that a rectifying barrier occurs at the junction of the P+ and N annulae will make the radial field component larger in the junction region and smaller elsewhere. Therefore, until the depletion extends to the silicon-sapphire interface, the one-dimensional approximation should be valid.

Figure 2.2 shows sketches of the assumed charge, electric displacement, and potential distributions. Surface charges at the Si-SiO_2 and Si-Sapphire interfaces are assumed. The existence of the former is well established, and the latter is required to prevent depletion of the interface when a two-dimensional model is used. The two-dimensional calculation discussed in Chapter 4 showed that the field due to the junction would penetrate the sapphire and deplete the more lightly doped interface. If one assumes the thermally generated carriers in this region are collected, this gives rise to a leakage current, due to generation in this low lifetime region, which is much in excess of that observed with small gate

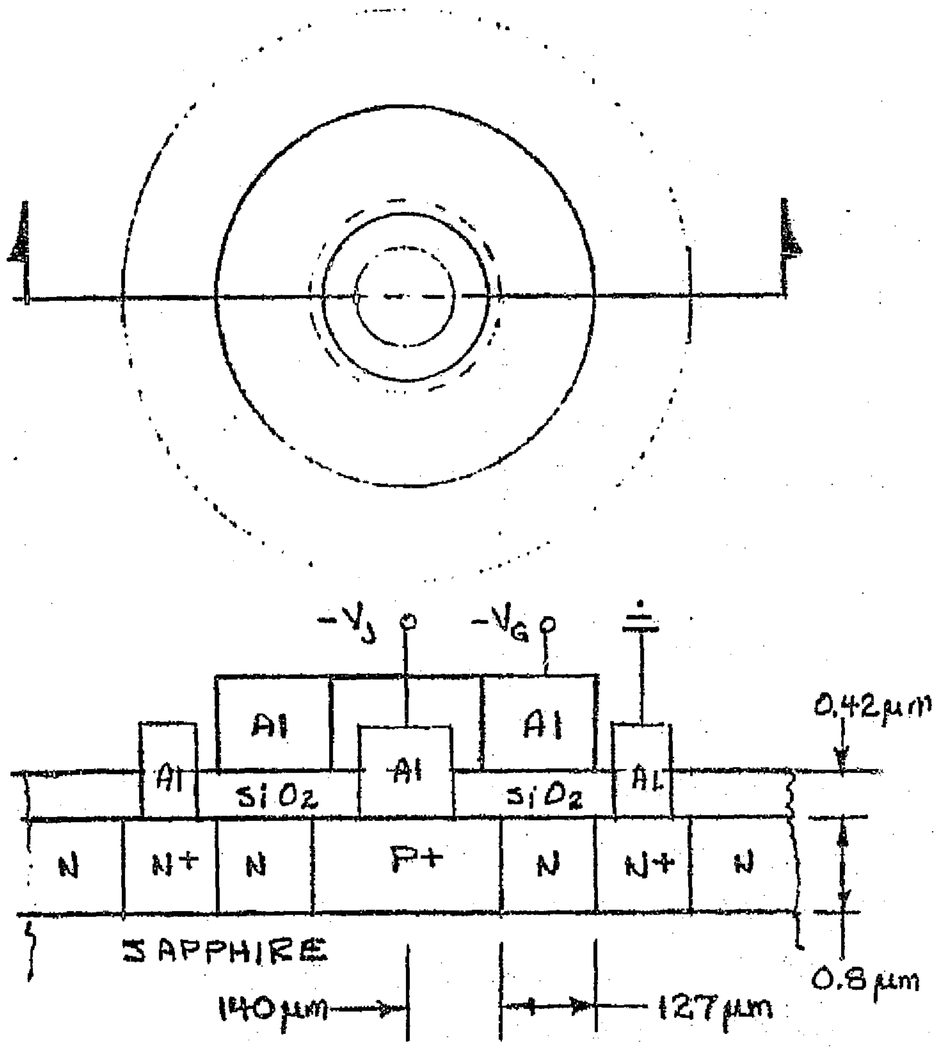

Figure 2.1 Geometry of SOS-GCD Structure

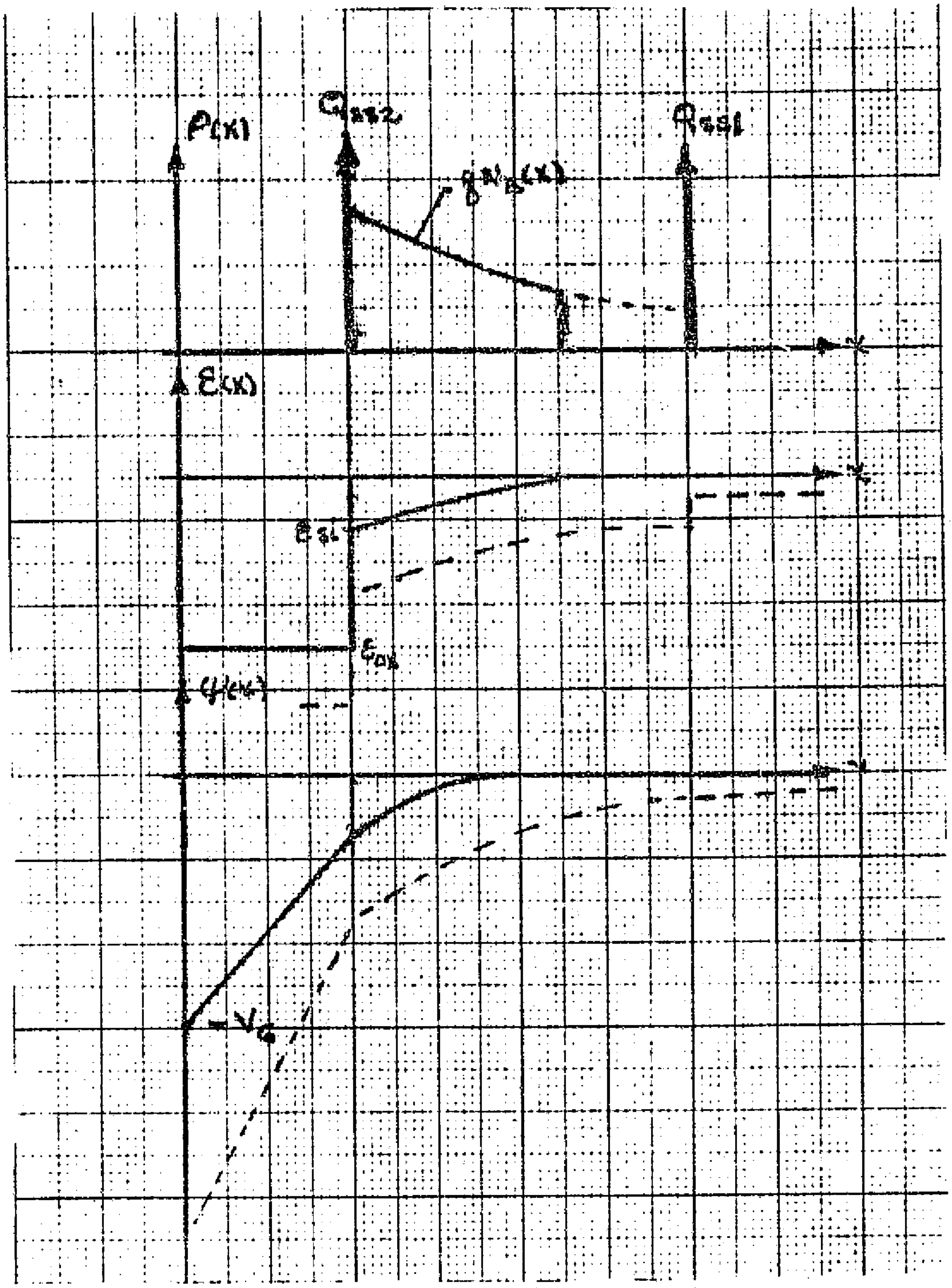

Figure 2.2 Charge, Field and Potential Distribution
Normal to surface of SOS-GCD

voltages. A fixed positively charged layer will keep the interface in accumulation until the field component due to the gate electrode depletes this region.

Application of the Poisson analysis to this problem is relatively straightforward. It is advantageous, however, to consider two cases, i.e., Case I, depletion is short of the Si-Saphire interface, and, Case II, depletion extends through the silicon film.

Case I. Depletion thickness less than film thickness.

$$\frac{dD}{dx} = \rho \qquad 2.1\text{-a}$$

$$D = D_{ox} \qquad 0 \leq x \leq t_{ox} \qquad 2.1\text{-b}$$

$$D = D_{ox} + Q_{ss2} + q \int_{t_{ox}} N_B(x)\, dx\,, \quad t_{ox} \leq x \leq t_{ox} + x_d \qquad 2.1\text{-c}$$

$$\frac{d\psi}{dx} = -\frac{D}{\varepsilon} \qquad 2.2\text{-a}$$

$$\psi(x) = V_G - D_{ox}\, x/\varepsilon_{ox} \qquad 0 \leq x \leq t_{ox} \qquad 2.2\text{-b}$$

$$\psi(x) = \psi_{xo} - (D_{ox} + Q_{ss2})(x - t_{ox})/\varepsilon_{si}$$

$$-\frac{q}{\varepsilon_{si}} \int_{t_{ox}}^{x} dy \int_{t_{ox}}^{y} N_B(z)dz$$

$$t_{ox} \leq x \leq t_{ox} + x_d \qquad 2.2\text{-c}$$

At the bottom of the depletion layer, $\psi(x_d) = 0$ and $D(x_d) = 0$. Therefore

$$D_{ox} = -q\int_{t_{ox}}^{t_{ox}+x_d} N_B(x)dx - Q_{ss2} \triangleq -(Q_B + Q_{ss2}) \qquad 2.3$$

$$\psi_{xo} = (V_G - D_{ox}/C_{ox}) = V_G + (Q_B + Q_{ss2})/C_{ox} \qquad 2.4$$

$$\Delta\psi = \frac{q}{\varepsilon_{si}}\int_{t_{ox}}^{t_{ox}+x_d} dy \int_{t_{ox}}^{y} N_B(z)dz \qquad 2.5$$

$$C_{si} = \varepsilon_{si}/x_d \qquad 2.6$$

$$C_{ox} = \varepsilon_{ox}/t_{ox} \qquad 2.7$$

We further define:

$$Q_B(x) \triangleq q\int_{t_{ox}}^{x} N_B(x)dx \qquad 2.8$$

$$\Delta\psi_x \triangleq \frac{q}{\varepsilon_{si}}\int_{t_{ox}}^{x} dy \int_{t_{ox}}^{y} N_B(z)dz \qquad 2.9$$

Then the potential is:

$$\psi(x) = V_G + (Q_B(x) + Q_{ss2})/C_{ox} + Q_B(x - t_{ox})/\varepsilon_{si} - \Delta\psi_x \qquad 2.10$$

For any depletion depth $x_d = x - t_{ox}$,

$$V_G = -(Q_B + Q_{ss2})/C_{ox} - Q_B/C_{si} + \Delta\psi \qquad 2.11$$

Equation (11) may be used to calculate the gate voltage required to deplete any arbitrary doping profile to the depth x_d. Note also that from (11):

$$dV_G = -(1/C_{ox} + 1/C_{si})dQ_B + d(\Delta\psi)$$

$$= -dQ_B/C_T + d(\Delta\psi) \qquad 2.12$$

where C_T is the measured gate capacitance.* Carrying out (carefully) the indicated differentiations with respect to x_d, one obtains:

$$N_B(x_d) = -\frac{C_T}{q}\frac{dV_G}{dx_d} \qquad 2.13$$

Further, from (6):

$$x_d = \frac{\varepsilon_{si}}{C_{ox}}\frac{(1 - C_N)}{C_N}$$

or,

$$x_d = \left(\frac{\varepsilon_{si}}{C_{ox}}\right)\frac{(1 - C_N)}{C_N}\ t_{ox} \qquad 2.14$$

where $C_N = C_T/C_{ox}$ is the normalized capacitance which could be obtained from measurements. Note that equations (13) and (14) provide a parametric pair which may be used to estimate the doping profile $N_B(x)$ for the depletion region giving rise to the capacitance C_{si} which is included in the measurement.

The leakage current due to generation of carriers in the depletion region of the field induced junction is simply given by:

$$\delta I_{gen} = qA\int_{t_{ox}}^{t_{ox}+x_d}\frac{n_i}{2\tau(x)}\,dx \qquad 2.15$$

or,

* less overlap capacitance.

$$\tau(x_d) = \frac{1}{2} qn_i/(\partial I_{gen}/\partial x_d) \qquad 2.16$$

Again (14) and (16) form a parametric pair for establishing the lifetime profile from junction current vs. gate voltage measurements if one assumes that the measured junction current, I_r, is equal to the generated current, I_{gen}. Figure 2.3 shows typical doping and lifetime profiles obtained by applying these parametric equations to Kranzer's data.

Case II. Full depletion of the silicon film.

In this case, only the regions for solution of (1-a) and (2-a) are extended. On the sapphire side of the si-saph. interface we have:

$$D_{sa} = D_{ox} + Q_{ss2} + Q_B + Q_{ss1} \qquad 1\text{-c}$$

$$\psi_{sa} = \psi_{xo} - (D_{ox} + Q_{ss2})/C_{si} - \Delta\psi \qquad 2\text{-c}$$

When this full depletion occurs, the field generally will be determined by boundary conditions and geometry so that ψ_{sa} will no longer be a constant value across the si-saph. interface. However, (1-c) and (2-c) may be used to establish the interface boundary conditions for a field solution in the sapphire region. Combining (1-c) and (2-c), we obtain:

$$\psi_{sa} = (Q_B + Q_{ss1} - D_{sa})/C_T + Q_{ss2}/C_{ox} + V_G - \Delta\psi \qquad 2.17$$

In the following, (2-17) is used in obtaining a numerical solution for the field in the sapphire when the through depletion occurs.

The equations obtained here can be used two ways. As pointed out, the pairs (13) - (14) and (14) - (16) can be used for analysis of experimental data as was done by Kranzer. If the profiles $\tau(x)$ and $N_B(x)$ are

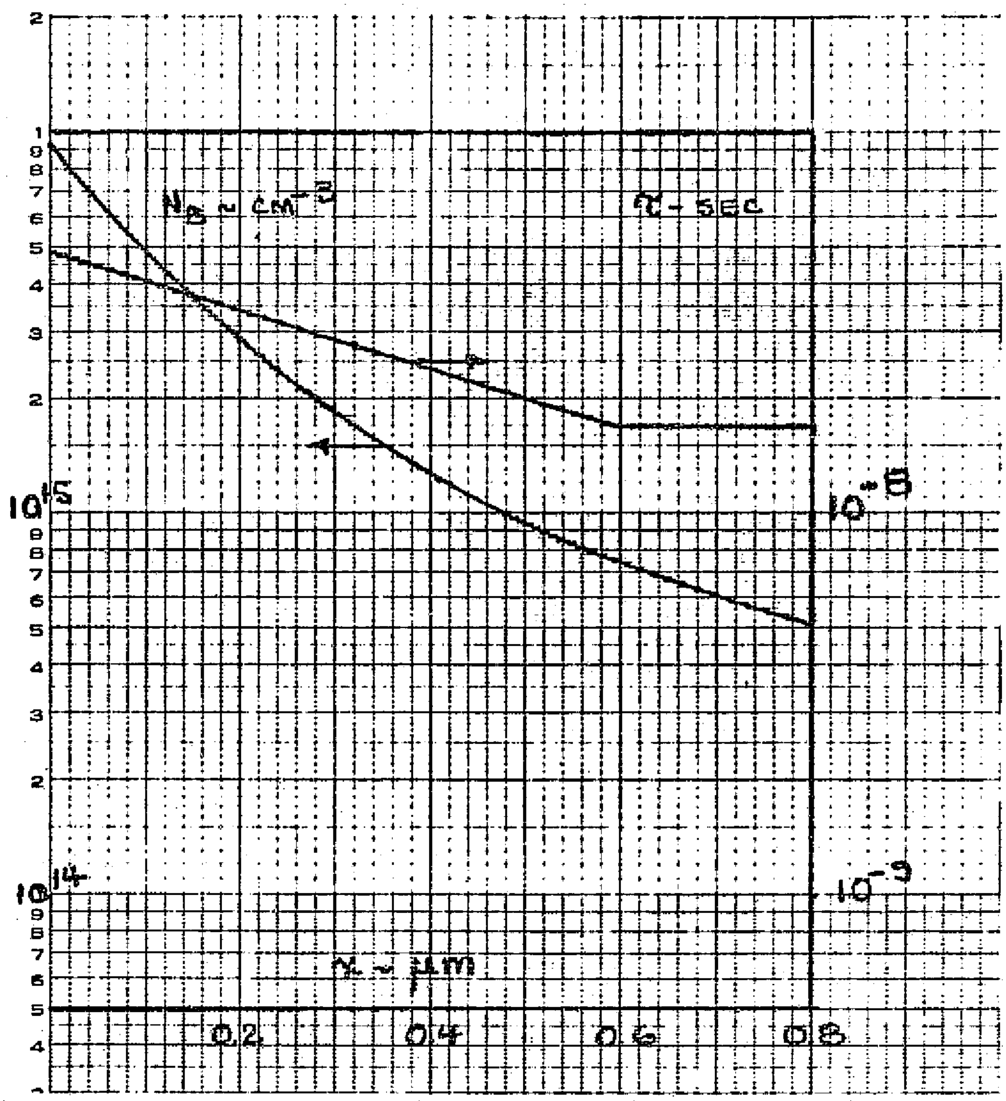

Figure 2.3 Doping and Lifetime Profiles in Silicon Film.

available, then (6), (7), (11) and (13) can be integrated (we use numerical methods) to obtain the capacitance voltage C_T vs. V_G (or C_N vs. V_G) and δI_{gen} vs. V_G curves.

CHAPTER 3

SIMPLIFIED TWO-DIMENSIONAL ANALYSIS

This work was done after that reported in Chapter 4; consequently, some insight into the electrical behavior of the GCD on SOS had been obtained. It was known that the 1-D depletion model gave a fairly good approximation before through-depletion if Q_{ssi} (the fixed charge at the Silicon-Sapphire interface, SSI) was large enough to prevent depletion from the bottom of the film upward. In this case, the depletion edge advances downward with increasing $|V_G|$ with the edge parallel to the film surface. It seemed plausible, therefore, that with $Q_{ssi}>0$ an electron accumulation layer would exist at the SSI and that this accumulation layer would be gradually reduced across the SSI as the gate voltage, $|V_G|$, increased. In the 2-D self-consistent depletion analysis (SCDA) discussed in Chapter 4, this type of behavior can be modeled; however, the program converges slowly when the gate field penetrates significantly into the sapphire substrate. Thus, it was not practical to use the program to calculate C-V and I-V curves and to change parameters such as the film thickness, geometry etc.

It was concluded that a simplified program might be useful, especially after through-depletion occured. In this program, the film parameters could be changed freely, e.g. Q_{ssi} was a point of prime interest. It was already known that large values of Q_{ssi} caused a large offset in the C-V curves which had not been observed experimentally.

Meyer[7] had observed small offsets and Heiman[8] had observed a lack of "through-depletion" (very large offsets) for deep depletion transistors. This behavior had been explained in terms of a layer of fixed charge within a high-resistance glassy interlayer between the silicon film and the sapphire substrate.[9,10] The fixed charge resulted from ionized impurities, which might be unintentional contaminants or (presumably) doping impurities introduced laterally through the layer from the P+ and N+ regions. If doping impurities are introduced, note that acceptors from the P+ region would reduce Q_{ssi} at the inner edge of the annular depletion capacitance and donors from the outer N+ region would increase Q_{ssi}. Therefore, the distribution for Q_{ssi} would generally increase from the inner radius to the outer radius. The simplified program allows the treatment of Q_{ssi} as a non-uniform distribution on the SSI. Such a phenomena could possibly explain the lack of a sharp drop in the C-V curves when through-depletion occurs.

The algorithm for the simplified model is as follows:

1. Starting with an assumed set of boundary conditions, typically with $\psi = 0$ on the si-sapph interface, solve for the potential field in the sapphire using a successive-over-relaxation procedure (SOR).
2. Calculate the electric displacement field, D, on the sapphire side of the interface. Calculate the D field on the silicon side of the interface with the assumed surface potential using the one-dimensional formulas in Chapter 2.
3. If $D_{sa} - D_{si} > Q_{ssi}$ at $r = r_i$ on the interface, assume that at this point the surface is depleted of free carriers

and use (2-17) for boundary condition at this point for a new SOR solution. Test each point before starting a new solution.

4. Repeat (1) through (3) until no additional points on the interface satisfy the inequality of (3).

5. Increment the boundary value, V_G, and repeat.

Additional criteria are included in the algorithm to account for inversion. For example, when applying (2-17), the surface potential, ψ_{xo}, tested to determine if $\psi_{xo} < V_J - 0.55 - (kT/q)\ \ln(N_B(1)/n_i)$ where $N_B(1)$ is the doping of the silicon film at $x = t_{ox}$. If the inequality is satisfied, then ψ_{xo} is set equal to the right hand side and the B. C. given by (2-17) is expressed in terms of ψ_{xo}.

3.1 The Simplified Analysis Program

The program listing is given in Appendix A. It consists of a main program for implementing the algorithm and three subroutines. One subroutine establishes the lifetime and doping distributions to be used in the calculation. A second subroutine explicitly specifies the steps used in the SOR calculation and tests the residual to determine the maximum value during one sweep through the field. The third subroutine outputs the field data for the sapphire region. The main program proceeds with, first, a calculation of the capacitances and junction current vs. the gate voltage before the through-depletion occurs. The results from these calculations allow the establishment of the validity of assumed lifetime and doping distributions for the model as well as the value for the $Si\text{-}SiO_2$ interface charge Q_{ss2}.

After the one-dimensional calculations, the gate voltage is incremented to a value sufficient for the gate field to penetrate the sapphire. Then the two-dimensional problem in the sapphire is solved repetitively for a sequence of gate voltages in order to determine the gate electrode charge and the incremental capacitance. The SOR solution is based on the Gauss' law principle applied at each grid point within a cylindrical region. This formulation is set forth in a general form in Chapter 4 where the dielectric discontinuities and variable grid spacing are considered.

3.2 Calculated Results for Capacitance and Junction Currents.

Figures 3.1 and 3.2 show the calculated results for the case where through-depletion is not acheived. Circles represent Kranser's data.[6] Such errors as exist result from manipulating the data since the program for conditions before through-depletion is based upon a self-consistent 1 - D model. The calculated capacitance included parasitics from the stray capacitance of the probe which is incompletely guarded and an overlap capacitance between gate and the P^+ region. The probe stray was measured and is approximately 1 pF. The gate - P^+ overlap at the Si-SiO_2 interface can be estimated from the intentional overlap (0.75 mils) designed into the structure, but the overlap at the gate P^+ edge on the SSI must be estimated. This overlap was adjusted to give the correct minimum capacitance. Scott etal[11] have discussed this overlap which is troublesome for fabricating SOS integrated circuits, since sufficient overlap produces a drain-to-source short circuit.

Figure 3.3 shows the calculated capacitance vs. gate bias for an entire range of V_g and two values of V_J. The dotted curve shows the results for a low, uniform value $Q_{ss1}/q = 7.5 \times 10^9$ cm^{-2} and the dashed curve shows the result for a larger uniform value $Q_{ss1}/q = 1.25 \times 10^{11}$.

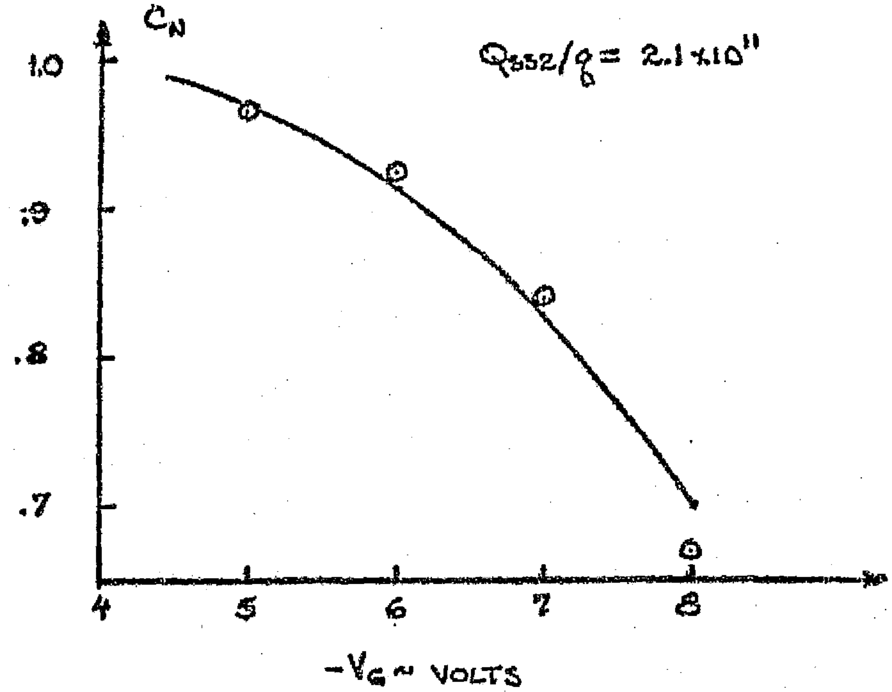

Figure 3.1 Gate Capacitance vs. Gate Bias

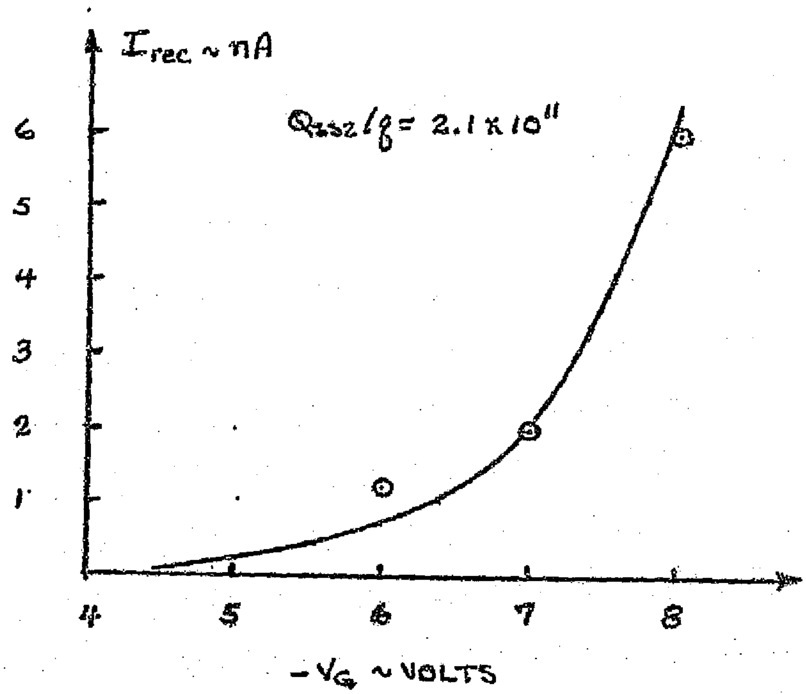

Figure 3.2 Junctic ı Current vs. Gate Bias

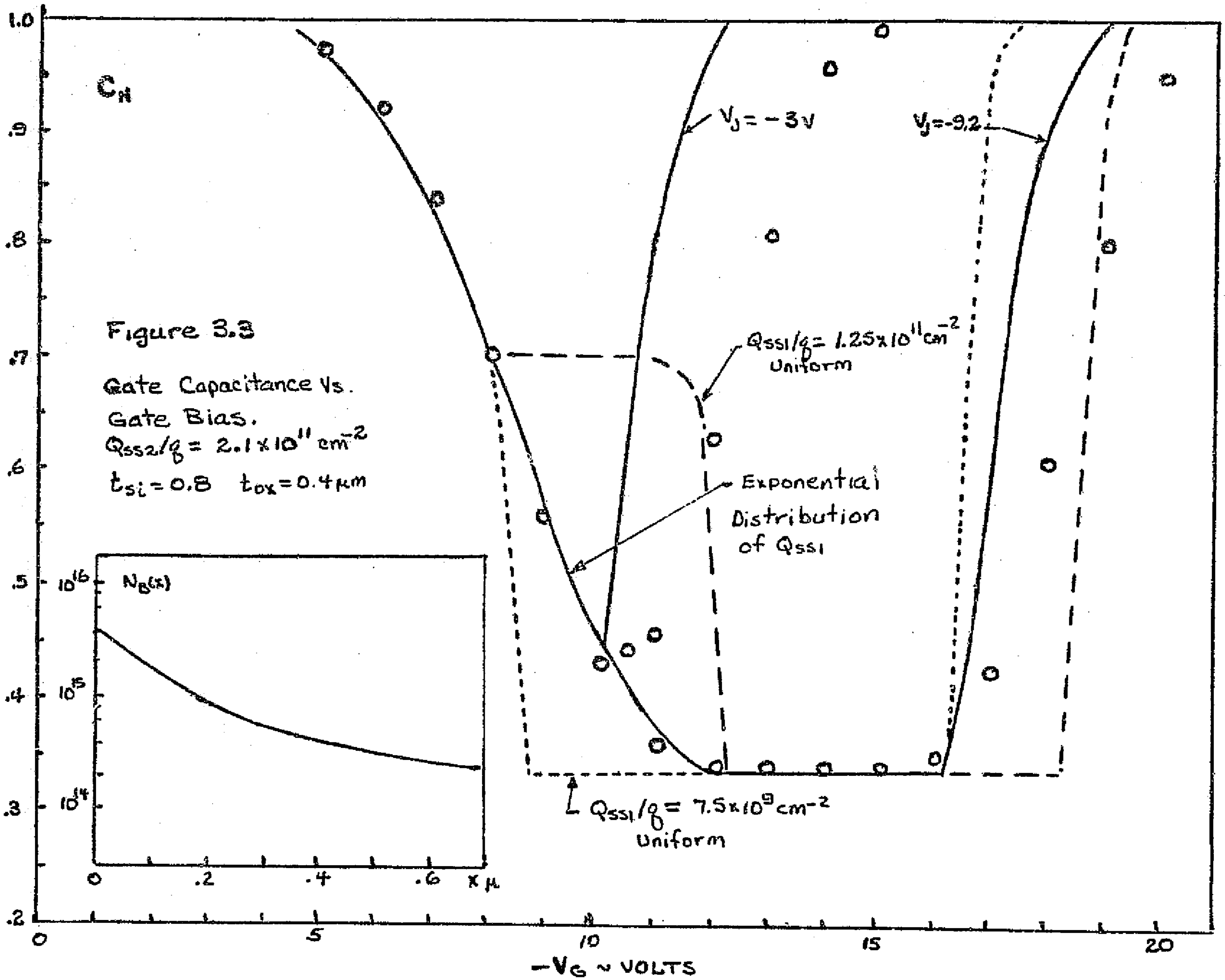

Figure 3.3

Gate Capacitance Vs. Gate Bias.

$Q_{SS2}/q = 2.1 \times 10^{11}\ cm^{-2}$

$t_{si} = 0.8 \quad t_{ox} = 0.4\ \mu m$

The solid curve is for an exponentially distributed Q_{ssi} with Q_{ssi}/q = 7.5×10^9 on the inner radius and $Q_{ssi}/q = 1.25 \times 10^{11}$ on the outer radius of the annular depletion capacitance. Obviously, a low uniform Q_{ssi} gives a sharp drop in C when through-depletion occurs while a large value of Q_{ssi} may give a noticeable offset (threshold for V_G) or may even preclude through-depletion before the inversion at the $Si-SiO_2$ interface occurs. The gradual reduction of C due to the gradual removal of the accumulation charge on the SSI due to Q_{ssi} can be explained by a non-uniform distribution of Q_{ssi} on the SSI.

Figures 3.4 and 3.5 show the influence of the charge Q_{ss2} (at the $Si-SiO_2$ interface) and the oxide thickness on the C-V curves. Figure 3.6 shows the increase in the junction current caused by generation on the SSI as the accumulation layer is reduced. The depletion model augmented by a surface generation model on the SSI can account for increases in current up to the point where the accumulation layer on the SSI is fully depleted. The surface recombination velocity used for the results in Figure 3.6 corresponds to an average lifetime of 2 n sec for a 0.1 micron layer. Experimentally, it is observed that the current continues to increase until inversion sets in, at which point the current falls off. The calculated field patterns discussed in the next section give some insight into what may be happening in the inversion region.

3.3 Calculated Field Patterns

Figure 3.7 shows equipotential surfaces in the sapphire for a through depleted condition while Figure 3.8 shows the normal electric flux density for a through-depleted and an inverted condition. In

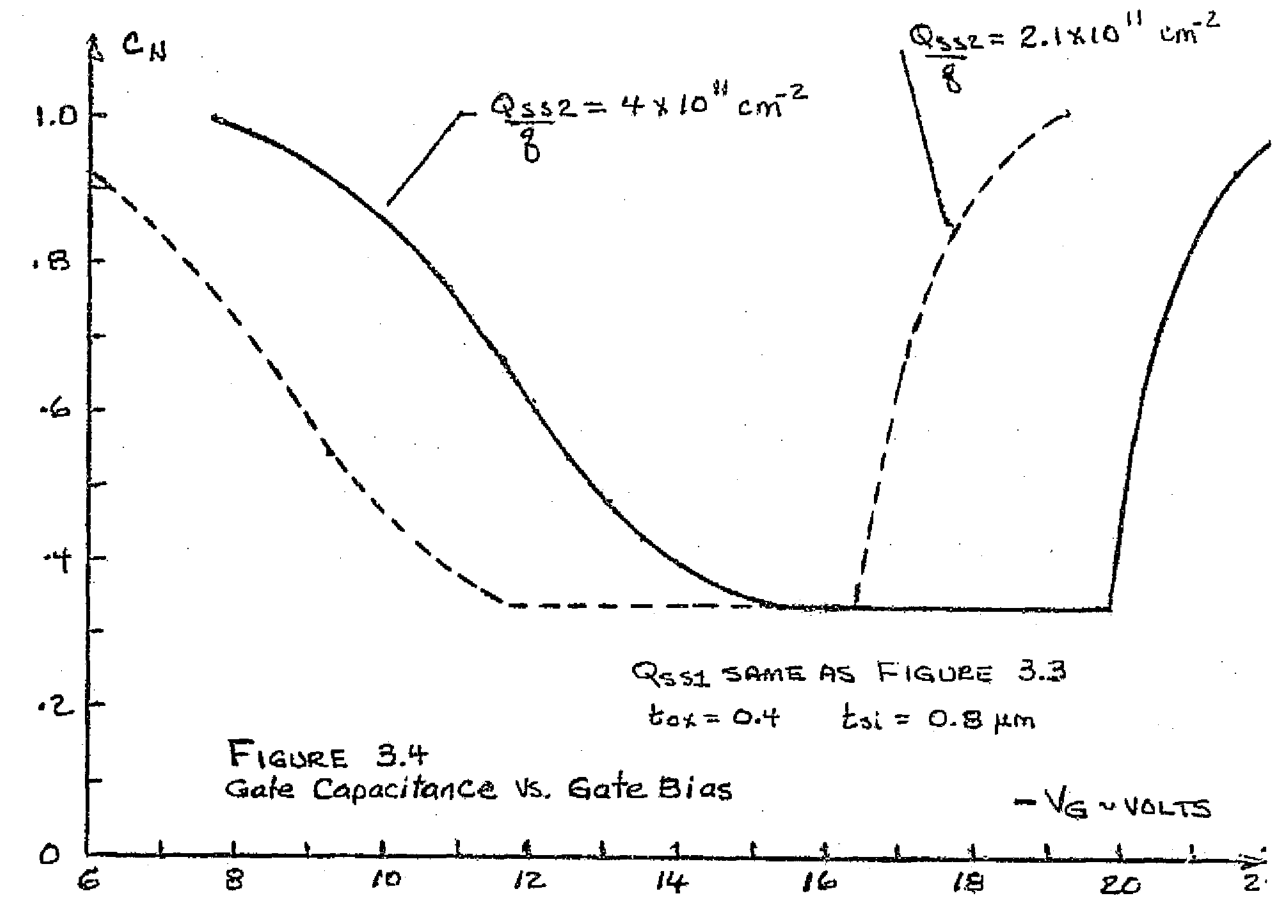

FIGURE 3.4
Gate Capacitance vs. Gate Bias

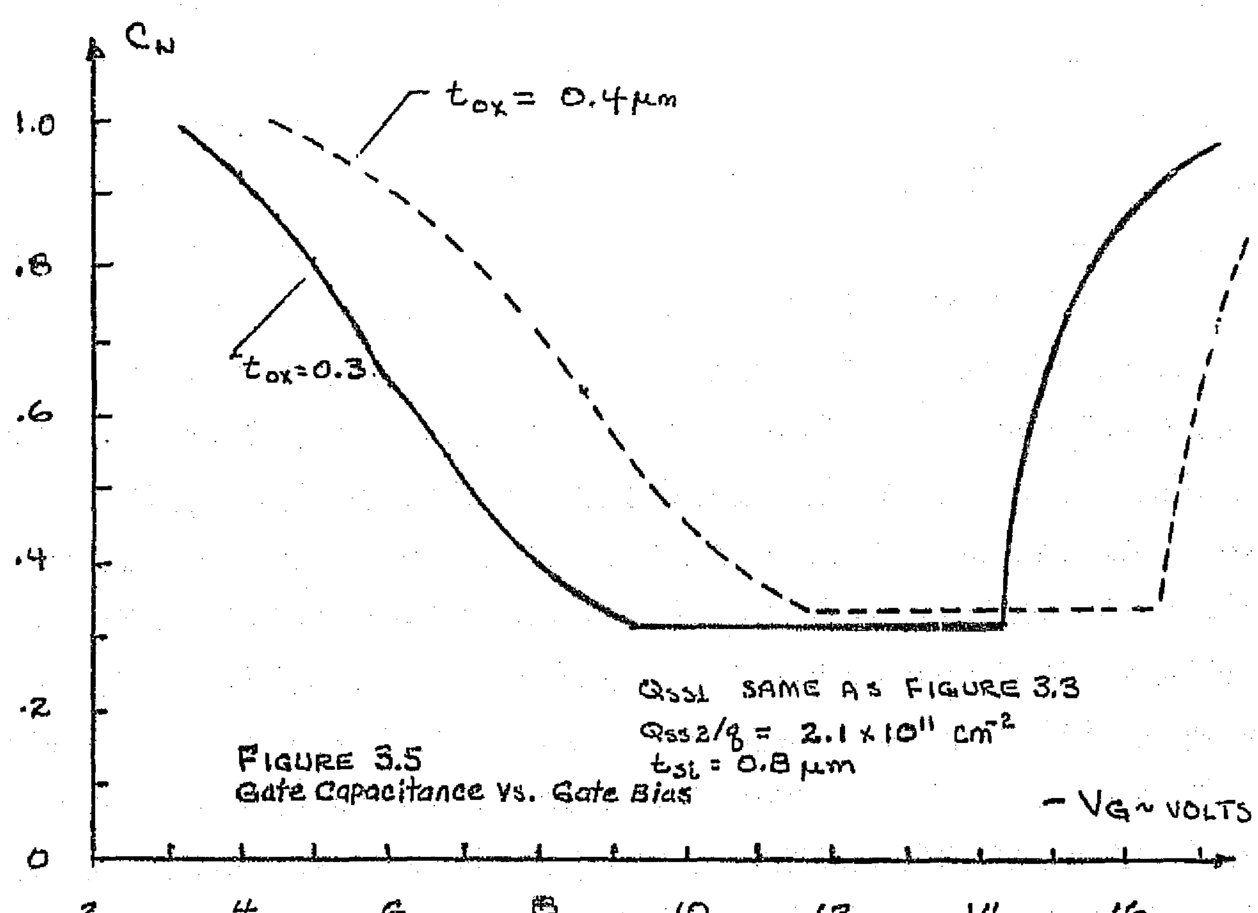

FIGURE 3.5
Gate Capacitance vs. Gate Bias

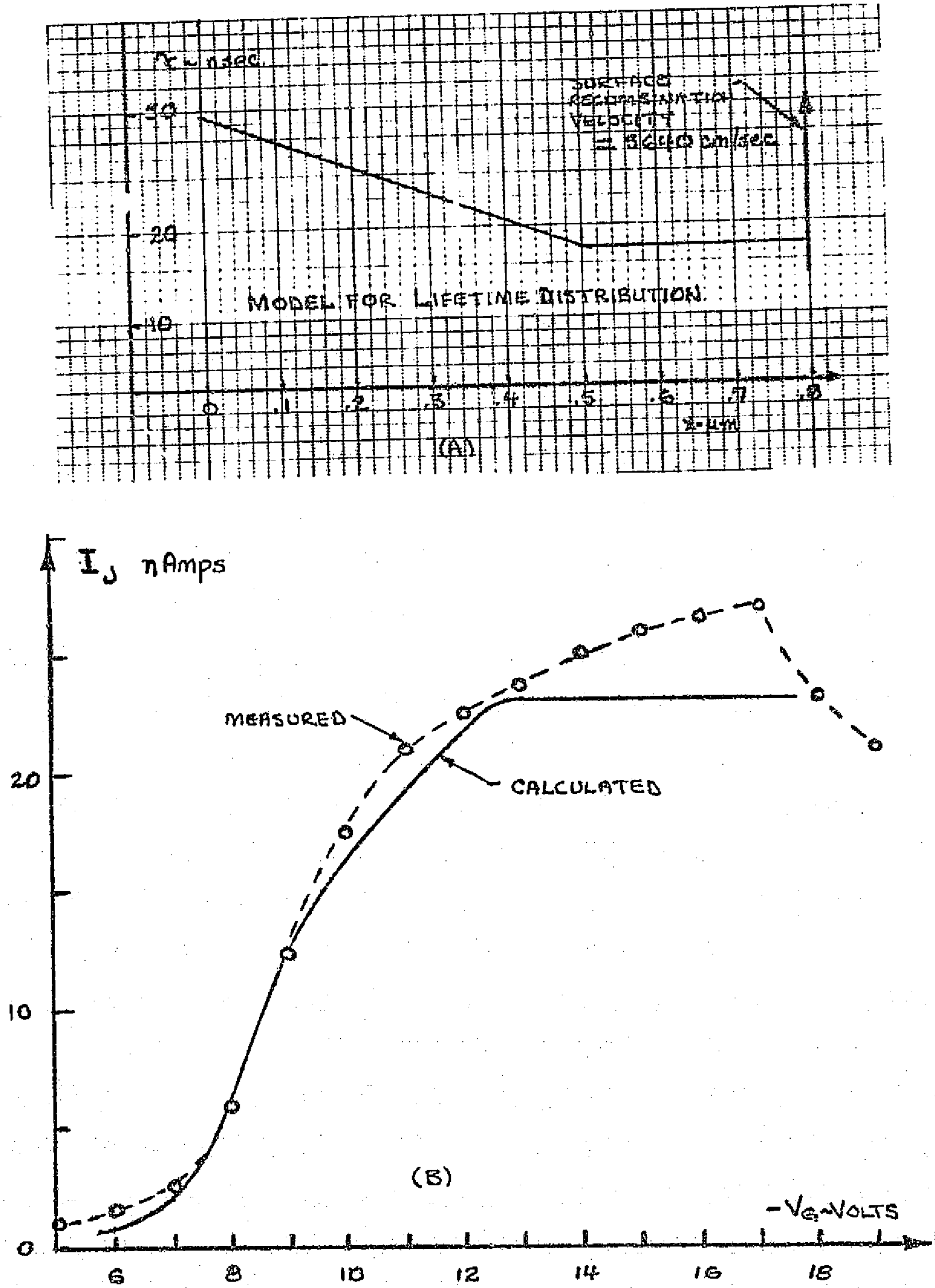

Figure 3.6 Junction Current vs. Gate Bias

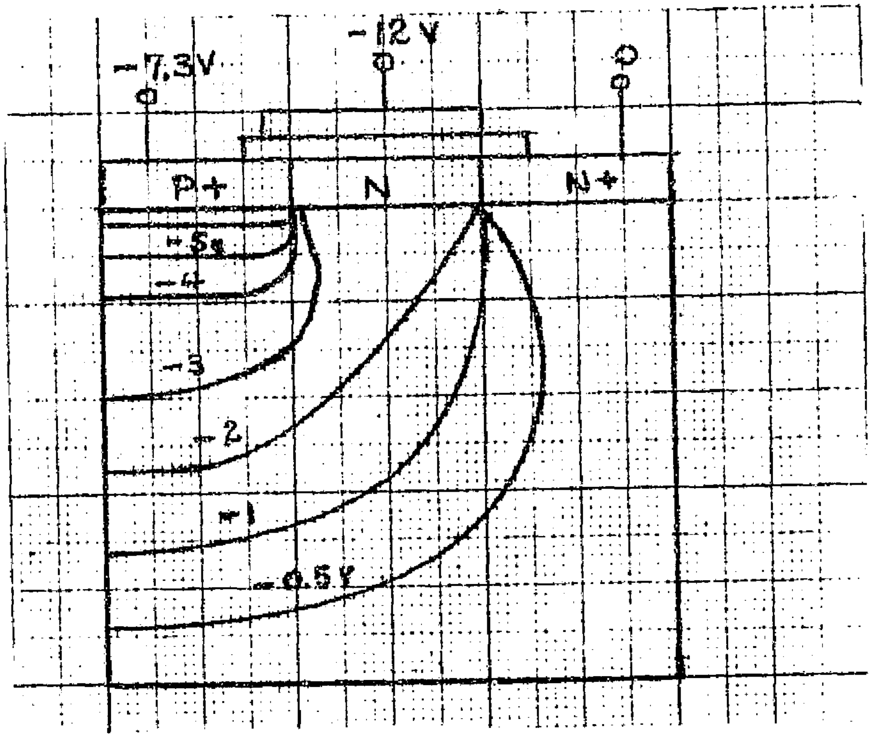

Figure 3.7 Equipotential Contours for Field in Sapphire

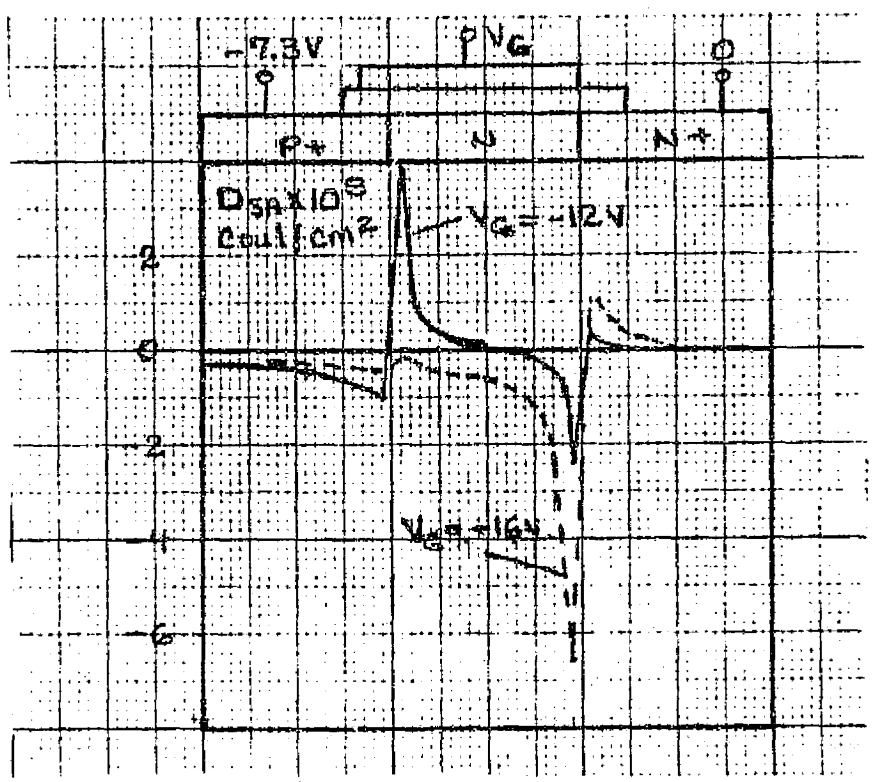

Figure 3.8 Normal Electric Flux Density on Silicon-Sapphire Interface

Figure 3.9 the radial field profiles along the silicon-sapphire interface are shown for three values of gate voltage. Note that the minimum field location shifts toward the P^+ region with increasing gate voltage. Collected hole current flows along the $Si-SiO_2$ interface while electron current flows on the SSI. At the center of the field, the electron current is approximately 10_{nA}, and if this current were confined in a layer 0.1 micron thick and the field value were 500V/Cm, the required electron density would be 10^{12} Cm^{-3}. This value would result in a channel resistance of approximately 100 Megohm; however, even this low a carrier density is significant in terms of recombination, since hole densities greater than $10^8 Cm^{-3}$ would result in net recombination. Apparently, all of the thermally generated carriers are not collected, and these may very well be those generated near the SSI. After the SSI is fairly well depleted, further increase in the gate voltage increases the radial field and results in an increase in the collection of the thermally generated carriers. However, when inversion sets in, the radial field drops substantially. This must be accompanied by an increase in the electron concentration on the SSI. Furthermore, the buildup of the hole concentration on the $Si-SiO^2$ interface will result in holes back diffusing toward the SSI. Therefore, it is quite plausible that this effect results in a decrease in the collected current with the onset of inversion. Figure 3.10 shows the integrated transit time from the P^+ to N^+ region along the SSI. Note the increase in this transit time as inversion sets in. Elementary arguments show that the total electron charge on the SSI must therefore increase accordingly or that the current must drop. The experimental results indicate a small drop in the current; therefore, the electron density must increase. The increase in the hole density due to back diffusion could then account for a reduction in the net thermal generation in the SSI region which results in a lower current.

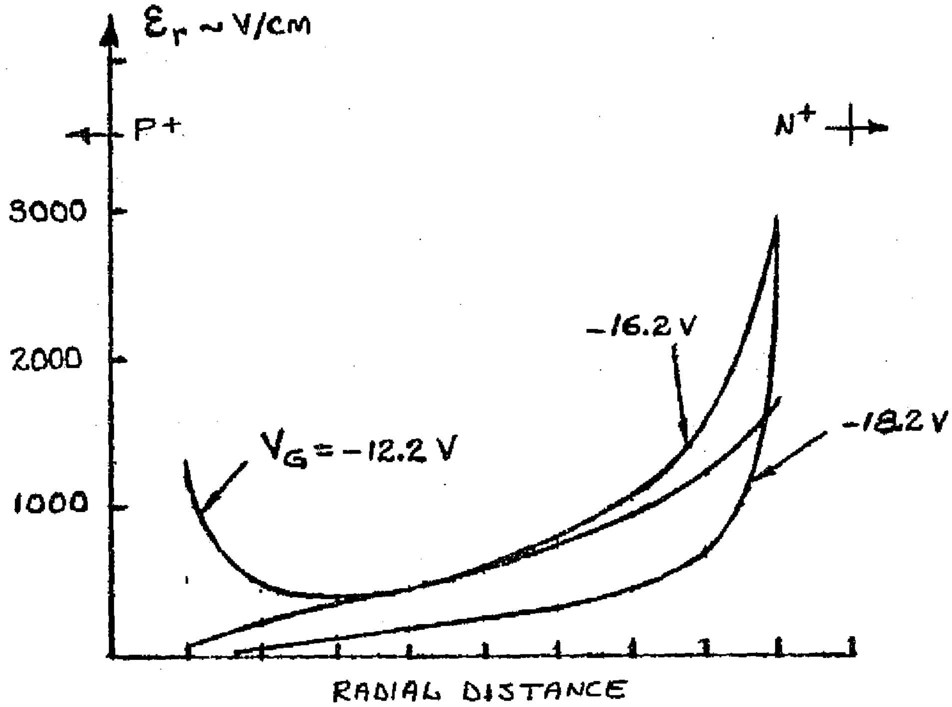

Figure 3.9 Radial Field Profiles along Silicon-Sapphire Interface.

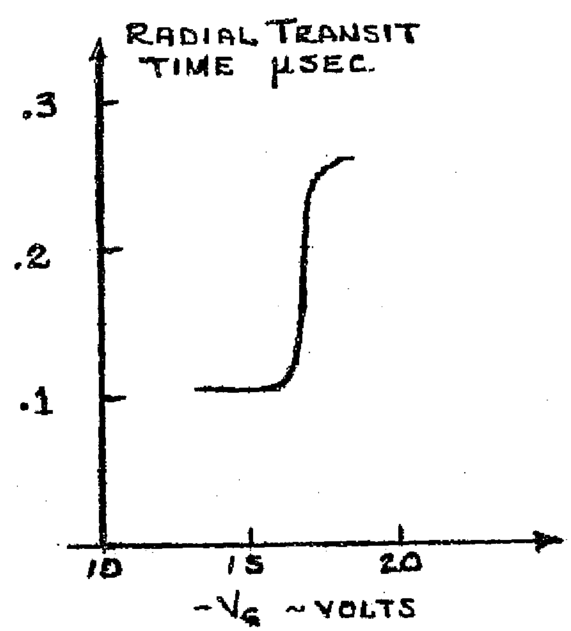

Figure 3.10 Radial Transit Time from N^+-N to P^+-N Junction.

3.4 Conclusions

The following conclusions were drawn from the results presented in this chapter.

1. The falling part of the C - V curve can be described with a 1-D depletion model before through-depletion and 2-D model afterward. Adjusting the intensity and distribution of the fixed charge Q_{ssi} allows the observation of three types of behavior:

   (a) a sharp drop in C at through-depletion if Q_{ssi} is small

   (b) An offset, or threshold for $|V_G|$, at through-depletion if Q_{ssi} is large. The offset may be large enough to prevent removal of the electron accumulation layer before inversion at the Si-SiO_2 interface occurs.

   (c) A continuous reduction of C, as ovserved by Kranser, may be obtained from a non-uniform distribution of Q_{ssi}. This type of distribution is plausibly the result of impurities diffusing laterally in the SSI from the P^+ and N^+ regions.

2. The minimum capacitance is dominated by the capacitances of the sapphire substrate, the gate - P^+ overlap, and the parasitic fields of the incompletely guarded probe and lead wire. All of these contributions are approximately equal.

3. The silicon film thickness has a small effect on the minimum capacitance observed. Small variations (±20%) in producing the the thin film would be difficult to detect.

4. The effect of the oxide thickness on the minimum capacitance is not large but is more significant than that of the silicon film.

5. The concept of a surface generation current on the depleted silicon-sapphire interface is useful in conjunction with the 1-D depletion model for calculating the I-V characteristic. The depletion model predicts too rapid a reduction of carrier density with increasing gate voltage near the SSI; hence the generation component increases too rapidly unless the lifetime is made artifically high. (See the level-off in Figure 2.3). Treatment of the reduction of the electron accumulation in terms of a surface layer for the final stage of depletion leads logically to the use of a surface generation velocity on the SSI.

6. When inversion occurs, the radial field component along the silicon-sapphire interface is substantially reduced. The radial transit time increases substantially; consequently there is an increase in the electron density on the SSI and a reduction in current. The reduction in current is probably due to the decrease in net thermal generation near the SSI because of the increase in the electron density and of the hole density due to holes diffusing back from the high concentration region on the inverted $Si\text{-}SiO_2$ surface.

Otherwise it was found that the modified program was efficient for economical generation of data and could easily be checked for convergence. It was found that for sapphire thicknesses in excess of 3 mils, the thickness or the boundary conditions, i.e. either zero normal field or zero potential, had little effect on the field in the film or on the calculated capacitance, current, etc.

CHAPTER 4

COMPLETE TWO-DIMENSIONAL ELECTROSTATIC ANALYSIS OF THE SOS-GCD

A more accurate cross-section diagram of Kranzer's[5,6] devices is shown in Figure 4.1 which shows that the gate electrode does not completely cover the annular N-region between the P+ and N+ diffusions. One would anticipate fringing effects because of the lack of overlap on the N+ edge, and that the fringing will be more significant as the silicon film is depleted to the sapphire substrate. A two-dimensional model within the film itself is necessary to account for the fringing and to investigate the transit time for the movement of thermally generated carriers from generation to sink sites.

Significant two-dimensional effects fall into two categories. (1) The effect of electrostatic field upon the determination of the gate capacitance is essentially a one-dimensional phenomena until the film is depleted through to the sapphire substrate. After through-depletion, the field has a strong two-dimensional character. (2) The small two-dimensional effect, as noted by a small radial field component in the depletion region, before the through depletion will have a significant effect upon the reverse current-gate bias relationship. Analysis of the problem must be done using numerical techniques. First, the appropriate equations must be formulated in a finite difference scheme, and then a suitable grid must be chosen to span the field of interest allowing the necessary resolution in critical regions.

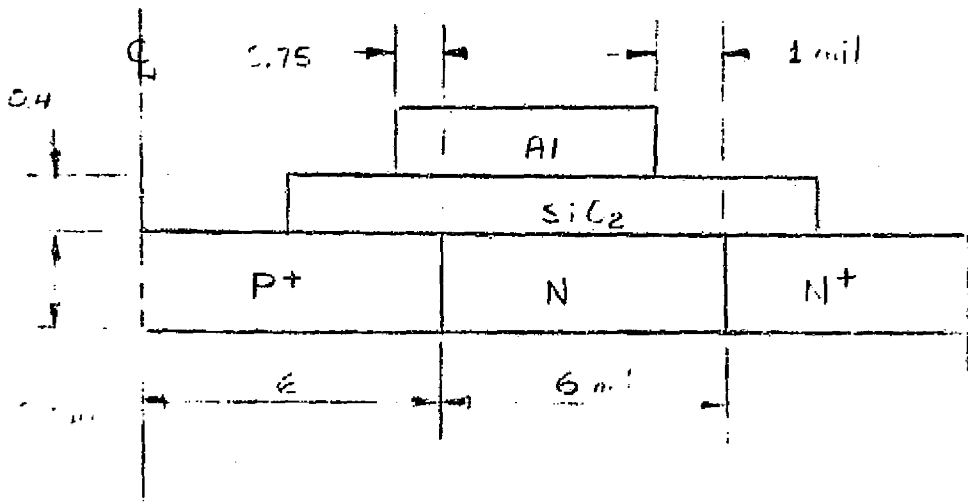

Figure 4.1 Cross-section of Gate-Controlled-Diode in SOS used by Kranzer.[6]

4.1 Electric Equations

It was assumed that the carrier velocity depended linearly upon the electric field, an assumption of dubious validity near the P+ N edge but reasonable otherwise. The current densities, $\bar{J}_p$ for holes and $\bar{J}_n$ for electrons are:

$$\bar{J}_p = -qD_p \nabla p - q\mu_p p \nabla\psi \qquad 4.1$$

$$\bar{J}_n = qD_n \nabla n - q\mu_n n \nabla\psi \qquad 4.2$$

The Shockley-Read recombination model was assumed so that the net recombination rate U is given by:

$$U = (pn - n_i^2)/[\tau_p(n + n_i) + \tau_n(p + n_i)] \qquad 4.3$$

with $\tau_p = \tau_n = \iota$, a function of z. Defining normalized fluxes $\overline{F}_p$ and $\overline{F}_n$ and generation rates G_p and G_n by:

$$\overline{F}_p \triangleq \nabla p + (\nabla\psi/V_T)p \qquad 4.4$$

$$\overline{F}_n \triangleq \nabla n - (\nabla\psi/V_T)n \qquad 4.5$$

where $V_T = kT/q$,

$$G_p \triangleq - G/D_p \qquad 4.6$$

$$G_n \triangleq - G/D_n \qquad 4.7$$

We then write the continuity equations as:

$$\nabla \cdot (\nabla p + (\nabla\psi/V_T)p) = G_p \qquad 4.8$$

$$\nabla \cdot (\nabla n - (\nabla\psi/V_T)n) = -G_n \qquad 4.9$$

These equations must be solved simultaneously with Poisson's equation:

$$\nabla \cdot (\varepsilon\nabla\psi) = - q(N_d + p - n) \qquad 4.10$$

The algorithm for a solution is based upon Gauss' theorem:

$$\oint_s \overline{F} \cdot \overline{n}ds = \int_v \nabla \cdot \overline{F}dv \qquad 4.11$$

Equation 4.11 is applied to each volume element in the grid. The appropriate volume element is a cylindrical ring of radius r_i, thickness Δr_i and height h_j . Normal fluxes, F_B, bottom, F_R, right, F_T, top, and F_L, left, at the elemental surfaces are expressed in finite difference form for holes as:

$$- F_B = \frac{P_{i,j} - P_{i,j-1}}{h_{j-1}} + \frac{\psi_{i,j} - \psi_{i,j-1}}{V_T h_{j-1}} \frac{(P_{i,j} + P_{i,j-1})}{2} \qquad 4.12$$

$$- F_L = \frac{P_{i,j} - P_{i-1,j}}{\Delta r_{i-1}} + \frac{\psi_{i,j} - \psi_{i-1,j}}{V_T \Delta r_{i-1}} \frac{(P_{i,j} + P_{i-1,j})}{2} \qquad 4.13$$

$$- F_R = \frac{P_{i,j} - P_{i+1,j}}{\Delta r_i} + \frac{\ _{i,j} - \ _{i+1,j}}{V_T \Delta r_i} \frac{(P_{i,j} + P_{i+1,j})}{2} \qquad 4.14$$

$$- F_T = \frac{P_{i,j} - P_{i,j+1}}{h_{j+1}} + \frac{\psi_{i,j} - \psi_{i,j+1}}{V_T h_{j+1}} \frac{(P_{i,j} + P_{i,j+1})}{2} \qquad 4.15$$

Applying Gauss' theorem:

$$\pi \frac{(r_{i+1} - r_{i-1})}{2} \frac{(r_{i+1} + 2r_i + r_{i-1})}{2} F_B + 2\pi \left(\frac{r_i + r_{i-1}}{2} \right) h_j F_L$$

$$+ 2\pi \frac{(r_i + r_{i+1})}{2} h_j F_R + \pi \frac{(r_{i+1} - r_{i-1})}{2} \frac{(r_{i+1} + 2r_i + r_{i-1})}{2} F_T$$

$$\cong -\pi \frac{(r_{i+1} - r_{i-1})}{2} \frac{(r_{i+1} + 2r_i + r_{i-1})}{2} h_j G_P \qquad 4.16$$

Defining:

$$\mathrm{ACR(I)} \triangleq (r_{i+1} - r_{i-1})(r_{i+1} + 2r_i + r_{i-1})/4 \qquad 4.17$$

$$\mathrm{BCR(I)} \triangleq (r_i + r_{i-1})/(r_i - r_{i-1}) \qquad 4.18$$

$$\mathrm{DCR(I)} \triangleq (r_{i+1} + r_i)/(r_{i+1} - r_i) \qquad 4.19$$

$$\mathrm{DCR(I)} \triangleq \mathrm{ACR(I)} \qquad 4.20$$

and,

$$\mathrm{AP} = \mathrm{ACR(I)}*H^{-1}*\left(1 - \frac{\psi_{i,j} - \psi_{i,j-1}}{2V_T}\right) \qquad 4.21$$

$$\mathrm{BP} = \mathrm{BCR(I)}*H*\left(1 - \frac{\psi_{i,j} - \psi_{i-1,j}}{2V_T}\right) \qquad 4.22$$

$$DP = DCR(I)*H*(1 - \frac{\psi_{i,j} - \psi_{i+1,j}}{2V_T}) \qquad 4.23$$

$$EP = ECR(I)*H^{-1}*(1 - \frac{\psi_{i,j} - \psi_{i,j+1}}{2V_T}) \qquad 4.24$$

where $H = h$ and $H^{-1} = 1/h$. Similar expressions are found for electron concentrations except that the drift term containing ψ has the opposite sign. These coefficients are AO, BO, Do and EO. Then:

$$CP = AO + BO + DO + EO \qquad 4.25$$

$$CO = AP + BP + DP + EP \qquad 4.26$$

Finally,

$$- AP*P_{i,j-1} - BP*P_{i-1,j} + CP*P_{i,j} - DP*P_{i+1,j} - EP*P_{i,j+1} = -ACR(I)*H*G_p \qquad 4.27$$

A similar expression is found for the electron concentration n.

In further work, a concession could be made to the nonlinearity of the drift velocity by testing the term $\Delta\psi/2V_T$ in calculating AP, BP, etc. If this quantity is greater than a saturation value, $v_{sat}*\Delta r/2V_T\mu$, etc. it could set equal to the saturation value with v_{sat} taken as 8.5×10^6 cm/sec and 4.4×10^6 cm/sec for holes and electrons respectively. Values of 5.2 and 13 cm^2/sec for the diffusion constants were bulk values, thus too high, and should be modified for further work.

Boundary conditions used were zero normal current at the Si-SiO_2 and Si-Saph interfaces and $J_{nr} = 0$ and $p = 0$ at the left edge and $J_{pr} = 0$ and $n = N_d$ at the right edge.

For the space charge equation 4.10, we proceed in a similar manner with additional defined terms which allow handling the discontinuity in ε, the permittivity:

$$AZ(J) = \varepsilon_{j-1}/(Z_j - Z_{j-1}) \qquad 4.28$$

$$BZ(J) = (\varepsilon_j(Z_{j+1} - Z_{j-1}) + \varepsilon_{j-1}(Z_j - Z_{j-1}))/2 \qquad 4.29$$

$$DZ(J) = BZ(J) \qquad 4.30$$

$$EZ(J) = \varepsilon_{j+1}/(Z_{j+1} - Z_j) \qquad 4.31$$

and,

$$Q_{i,j} = ACR(I)*H \times q(N_d + p - n) + ACR(I)*Q_{si,j} \qquad 4.32$$

where Q_s is a surface charge distribution such as Q_{ss1} and Q_{ss2} on the interfaces. Then,

$$A_{i,j} = ACR(I)*\ AZ(I) \quad \text{etc.} \qquad 4.33$$

So that we have

$$- A_{i,j}\psi_{i,j-1} - B_{i,j}\psi_{i-1,j} + C_{i,j}\psi_{i,j}$$

$$- D_{i,j}\psi_{i+1,j} - E_{i,j}\psi_{i,j+1} = Q_{i,j} \qquad 4.34$$

where $$C_{i,j} = A_{i,j} + B_{i,j} + D_{i,j} + E_{i,j}$$

The boundary conditions applied are best illustrated in the drawing of the grid system shown in Figure 4.2.

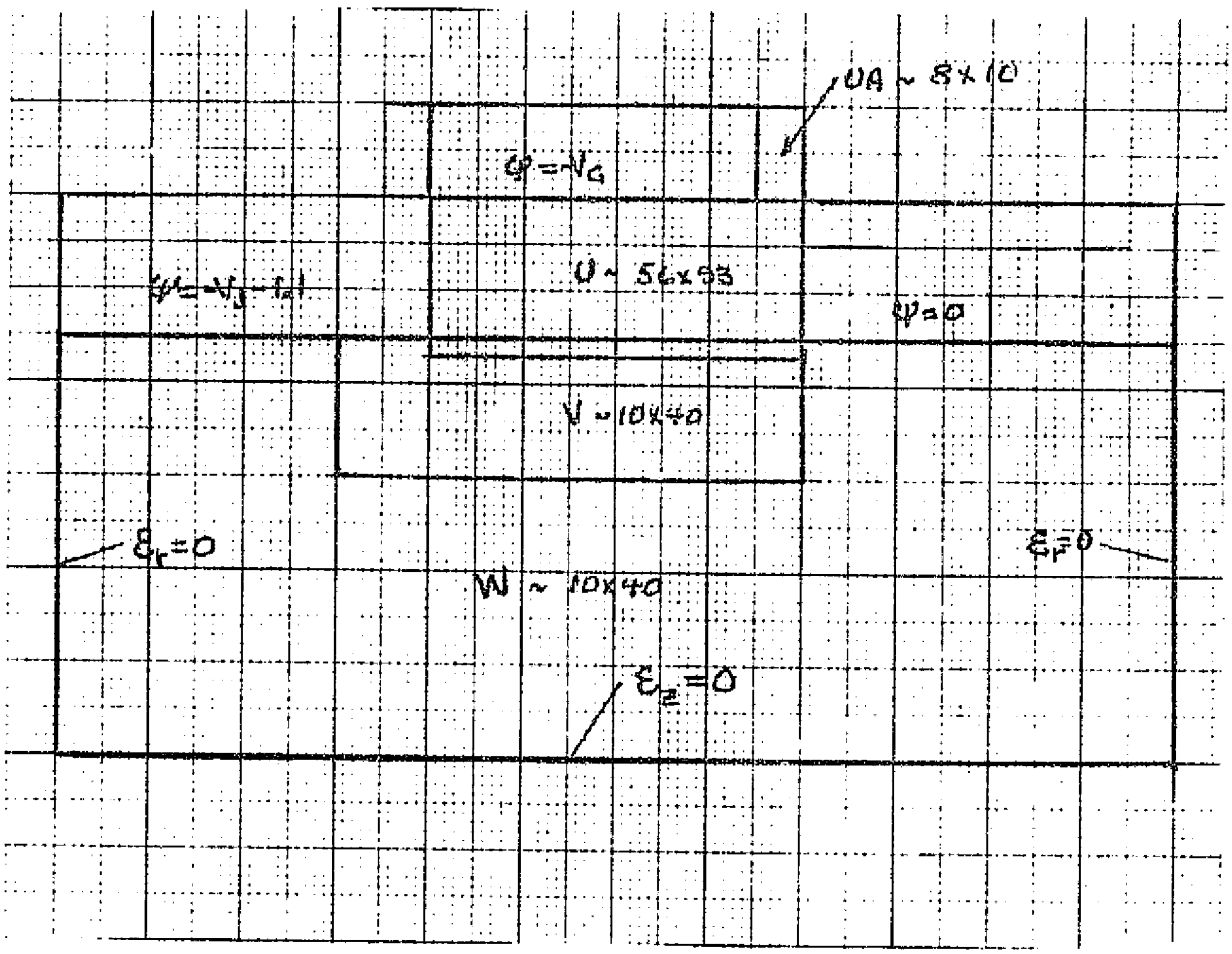

Figure 4.2 Diagram of Interlinking Fields

4.2 The Grid System

Choice of a reasonable grid system is the most challenging task in the analysis. One needs a fine grid within the silicon film to determine the small fields which exist before through depletion. However, if this is extended into the sapphire, an unreasonably large number of grid points is required to span a sufficiently large region in the sapphire. The accuracy of the field determination in the sapphire influences greatly that of the field in the film, particularly after through depletion. Figure 4.2 illustrates how the problem was approached. A 92 x 56 point + 8 x 10 point mesh was established to cover the films and air space over the naked oxide and a thin region within the sapphire. Then a 10 x 40 points mesh was selected to cover the sapphire. A linking mesh of 10 x 40 points was chosen for interpolation between interior points of the meshes and their boundaries. The respective field are U + UA, V, and W.

The radial spacing in the U field is non-uniform to allow a finer mesh near the P + N junction. The Z spacings in the V and W fields are non-uniform with a finer mesh near the upper boundaries. An exponential type spacing is used.

4.3 The Algorithm

The system of equations is solved using the Gauss-Seidel method with a relaxation parameter ω. At the end of the nth iteration, the field and carrier concentrations have been estimated at all field points. The (n + 1)th estimate for ψ, for example, is obtained as:

$$\tilde{\psi}_{i,j} = (A_{i,j}\psi^{n+1}_{i,j-1} + B_{i,j}\psi^{n+1}_{i-1,j} + D_{i,j}\psi^{n}_{i+1,j} + E_{i,j}\psi^{n}_{i,j+1} + Q^{n}_{i,j})/C_{ij} \qquad 4.35$$

$$\psi^{n+1}_{i,j} = (1 - \omega)\, \psi^{n}_{i,j} + \omega\, \tilde{\psi}_{i,j}$$

where $0 \le \omega < 2$ and typically $\omega \cong 1.7$.
The equations for $P_{i,j}$ and $n_{i,j}$ may be solved in a similar manner. The indicated sweep is from the left bottom corner, across and up through the field to the top right hand corner. After a sweep is completed, the order for the next sweep can be chosen to be different. The sweep order simply depends upon the start and end indices on two nested DO loops, and changing these corresponds to switching the superscripts n and n+1 in (4.35).

After a sweep through the field, all of the coefficients, $A_{i,j}$, $AP_{i,j}$, $AO_{i,j}$, etc., $G_{i,j}$ and $Q_{i,j}$ are calculated in terms of present estimates. Then the next sweep of the relaxation procedure is carried out. The iterative process is terminated when the selected residuals $\Delta\psi$, Δp or Δn are within the bounds prescribed.

4.4 Discussion of Program Operation

It was realized that the computational problem was very large. Initially the program was developed so that $Q_{i,j}$ was calculated using a depletion model, i.e. $\rho_{i,j} = qN_d$ for $\psi_{i,j} < kT\, \ln(N_d/n_i)/q$ and $\rho_{i,j} = 0$. Otherwise the potential was limited at $kT\, \ln(N_c/n_i)/q$. For the depletion model, approximately 8 minutes of CPU time (UNIVAC 1106) was required for satisfactory convergence without through-depletion. The procedure required 800 iterations and resulted in a potential residual on the order of 1mV. When through depletion occurred, the residual was on the order of 15 mV and decreasing slowly after this number of iterations. This convergence was poor for calculation of the incremental capacitance since the differences in two field distributions were involved. For obtaining semiquantitative descriptions of the field, the results were adequate.

It was easy to include the continuity equations into the program. The relaxation procedure for p and n was carried out prior to calculating $Q_{i,j}$ which utilized these values. The program listing in Appendix B includes this feature. After computation of $Q_{i,j}$, the relaxation of the potential ψ was carried out. The results from this procedure were neither surprising nor encouraging. After 20 minutes of computation time, the convergence was poor. Qualitative features of the fields were reasonable; however, from a quantitative standpoint it was obvious that perhaps 1 hour of computational time would be needed to establish an accurate solution for one set of boundary conditions. Therefore, use of the program for modeling to calculate C-V and I-V curves for different doping and lifetime distributions was out of the question.

Subsequently the program was modified leaving out the continuity equation. The space charge was calculated as discussed above, after an alternative scheme was tried and ruled out. In the alternative scheme the space charge was calculated using an exponential formula involving the potential. This scheme was discussed in a preceding report.[4] This method increased the computing time too much for a dubious contribution to the accuracy.

After the fields are calculated using the depletion approximation for the space charge, the charge on the gate electrode, Q_{EL}, in the substrate, Q_{SIL}, and the current, I_{SIL}, are computed from sums approximating the appropriate integrals:

$$Q_{EL} = \int_{S_1} \overline{D} \cdot \overline{n}\, ds \qquad 4.37$$

$$Q_{SIL} = \int_V \rho\, dv \qquad 4.38$$

$$I_{SIL} = \int_V q\, G\, dv \qquad 4.39$$

where S_1 is the surface of the Si-SiO_2 interface and V is the volume of the n-region.

Note that in using the depletion approximation $G = n_i/2\tau$ and no recombination in the space charge region is allowed. This causes some difficulties as we shall see later.

4.5 Discussion of computed Results

In Figure 4.3 the concentration and potential profiles along a cylindrical surface approximately midway between the P + N and NN+ junctions are presented. The convergence of the calculation was poor, showing inconsistencies in the radial field distribution for the concentrations given by the solution. Nevertheless, the qualitative results are interesting. The gate voltage is -10V which corresponds experimentally to the condition for through depletion, although through-depletion is not shown here. The solution shows a significant pile-up of carriers near each interface, with the pile-up of electrons at the Si-sapph. interface being of particular interest. In this region the lifetime is very low in the model used, and while the hole concentration is low, the pn product is high enough for significant recombination to occur. The calculated current for this condition is approximately 14nA in fair agreement with the 18nA measured by Kranzer, and certainly dramatically better than

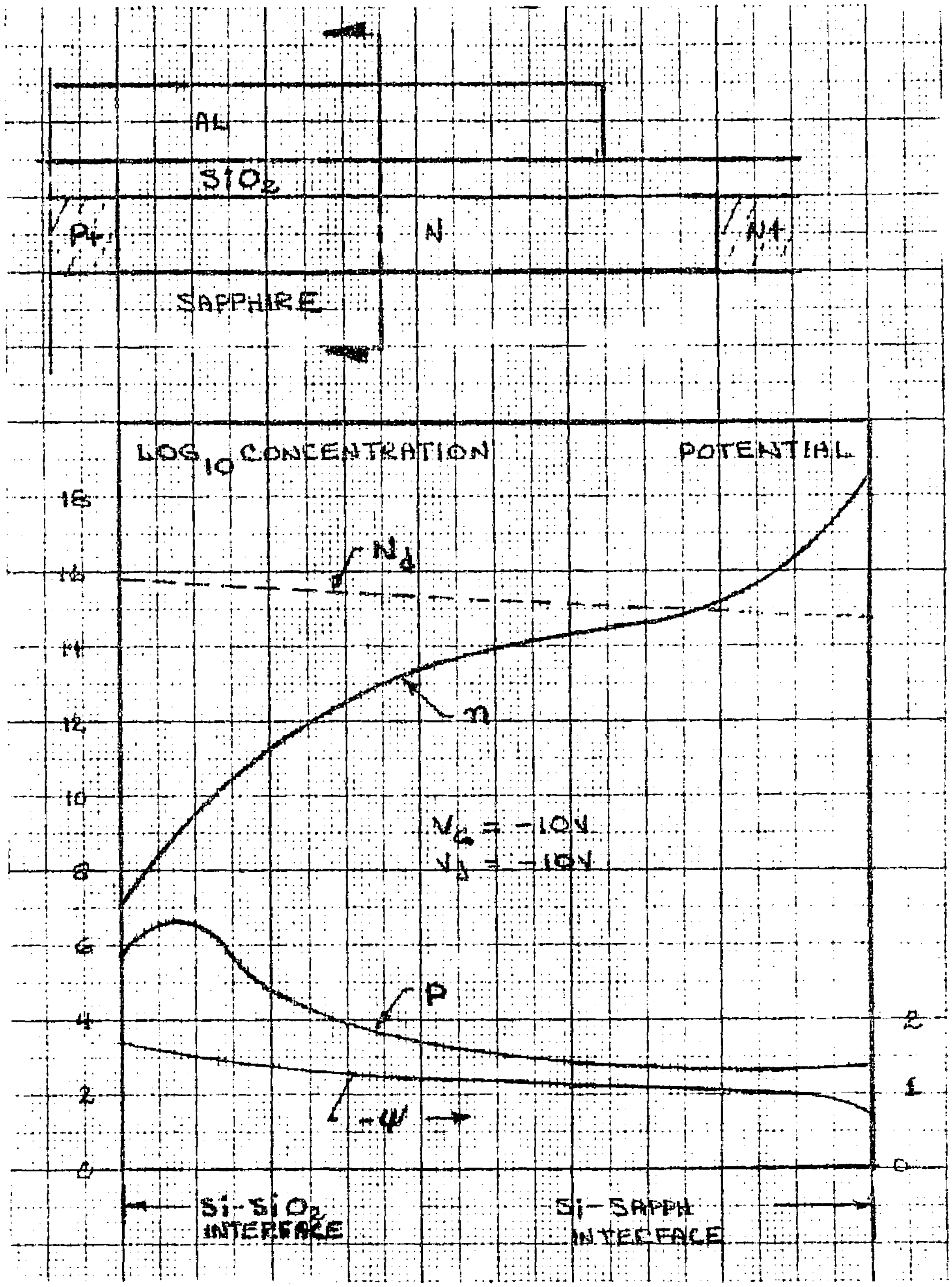

Figure 4.3 Carrier Concentration, Doping, and Potential Profile.

succeeding results using the depletion model. The location of the zero space charge surface is in fair agreement with the depletion edge found later using the depletion approximation.

After the program was modified deleting the continuity equations, it was run for a series of gate voltage values and for different values of surface charge, Q_{ss1}. Figures 4.4 and 4.5 show the depletion edges for two different values of Q_{ss1}, the si-sapph. interface. Figure 4.4 shows that, with $Q_{ss1} = 0$, the field from the sapphire due to the P+N junction penetrates the film. Qualitatively this is what one expects, with a significant penetration into the lightly doped silicon near the interface ($2.6 \times 10^{14} cm^{-3}$ doping at the interface). One should keep in mind that the horizontal scale is over 150 times the vertical scale when interpreting the graph. Figure 4.5 shows that for $Q_{ss}/q = 2.67 \times 10^{11}$ the depletion edge remains parallel to the $Si\text{-}SiO_2$ interface advancing into the film.

The calculated capacitances for the results in Figures 4.4 and 4.5 did not agree with the qualitative pictures of the depletion edge given. The convergence of the potential calculation was suspect and the number of iterations was increased to 800 per point where the starting solution taken was the solution for the last gate bias value. In Figure 4.6 the left hand curves were obtained in this way. The agreement of curve B with Kranzer's data was encouraging. Circles indicating his data were obtained from his normalized capacitance curve[6] using the maximum calculated value of 13.9 pF. Curve A, with the larger value of Q_{ss1}, shows the same offset that was observed in the simplified two-dimensional analysis. The disagreement at the left knee was attributed to the crude description of the doping profile and the Q_{ss2} value chosen to compensate

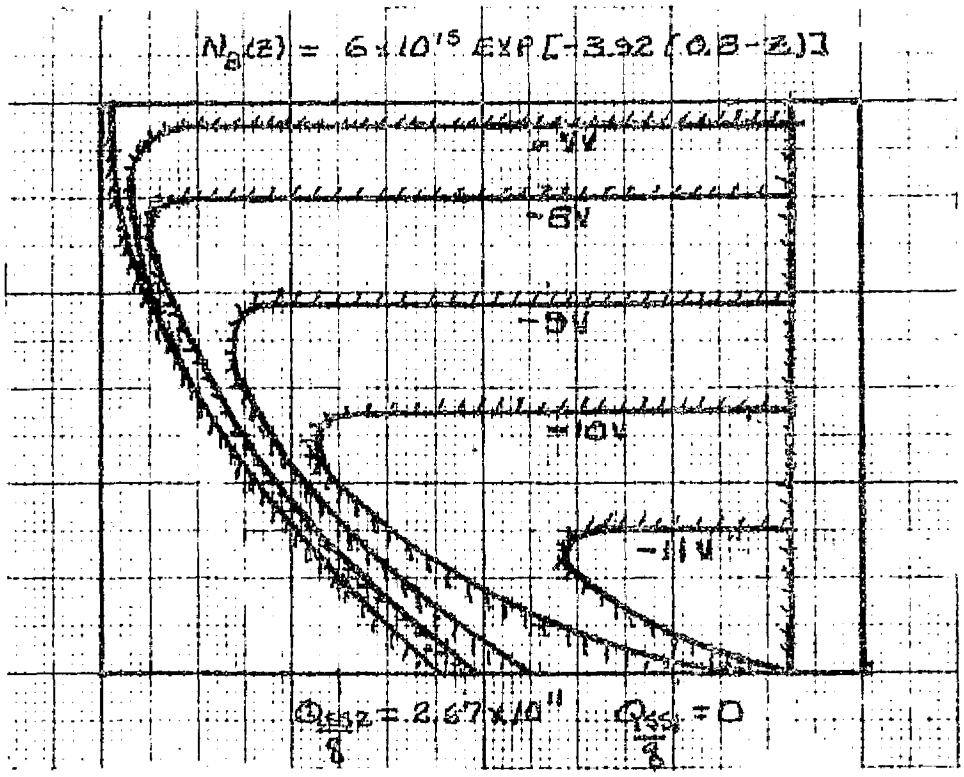

Figure 4.4 Depletion Edge Contours.

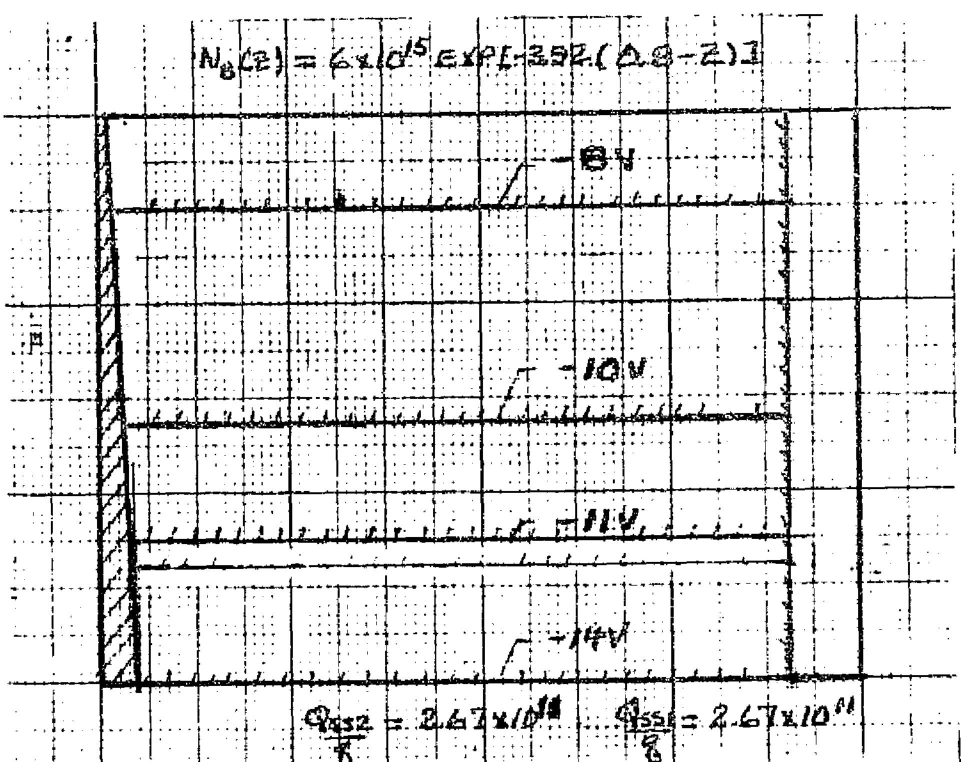

Figure 4.5 Depletion Edge Contours.

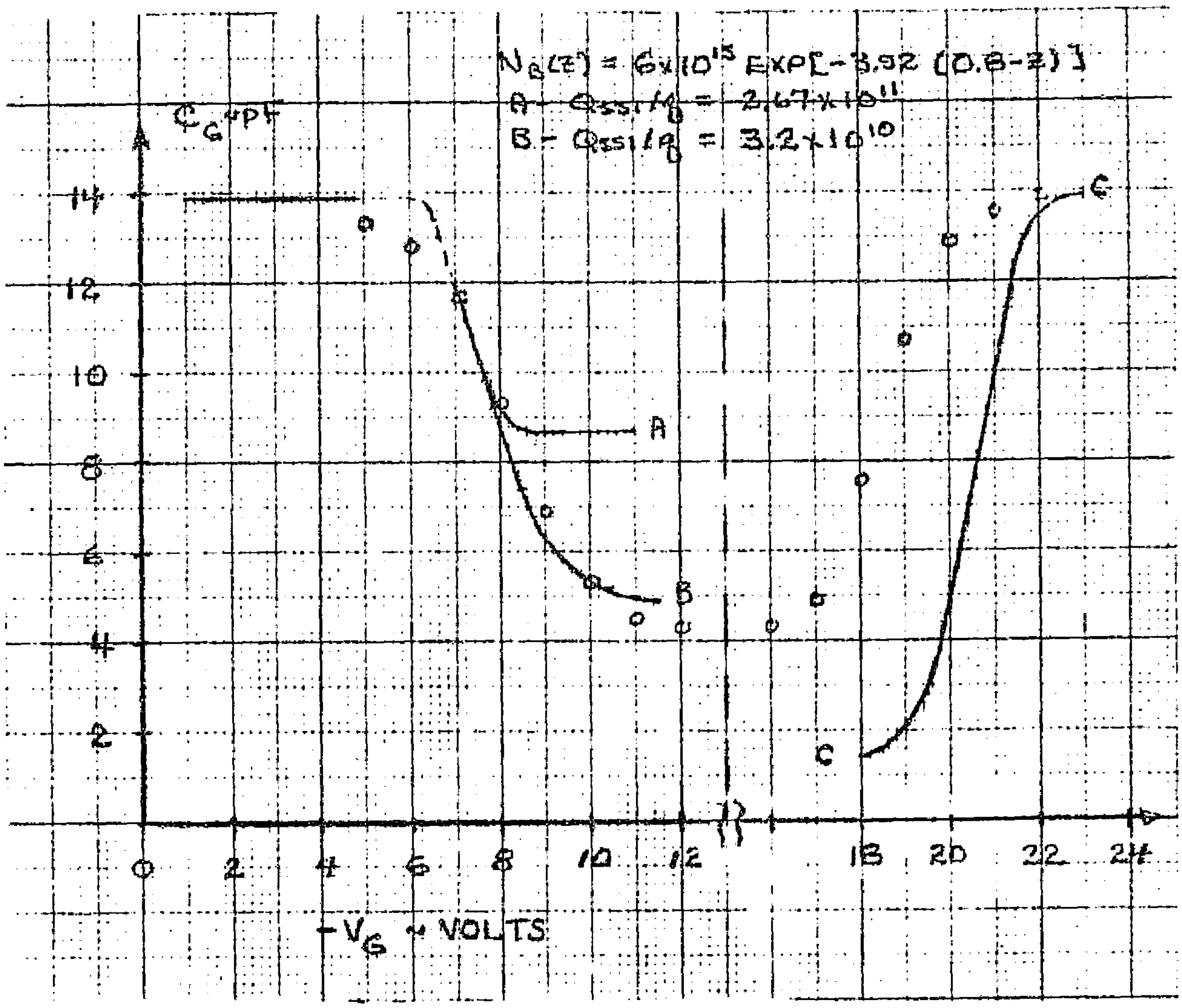

Figure 4.6 Gate Capacitance vs. Gate Bias $Q_{ss}/q = 2.67 \times 10^{11}$

See text for discussion of curve C.

this. Convergence problems were suspected because the calculated curve leveled off above the data, since this was observed before. A determination of the capacitance for $-15 < V_G < -14$ V then indicated a value of less than 3 pF with the capacitance falling with the number of iterations. This fell well below the data. Then the solution was started again at $V_G = -17$V where the capacitance curve should rise again. The calculation was run for 1800 iterations before a change was made in V_G to determine the capacitance. Then V_G was incremented in one volt steps and 800 iterations were made per point. The results were perplexing since the beginning capacitance value was 1.5 pF, far below the observed data. Otherwise the curve was shifted to the right of the data which could be accounted for because of improper values for Q_{ss2}, Q_{ss1}, $N_B(x)$, t_{si}, etc. Curve C in Figure 4.6 shows these results. At this point it had not been discovered that the capacitance calculation had not allowed for a significant overlap capacitance between the gate and p+ junction. The low value, 1.5 pF, agrees well with the value obtained with the simplified model without overlap.

There was a gross discrepancy between the calculated current, shown in Figure 4.7, and the current measured by Kranzer.[6] A major part of the difficulty was the lifetime model which was an exponential extrapolation of Kranzer's curve[5] which should be a reasonable description near the Si-SiO_2 interface. The "effective lifetime" fitting the I-V data to full depletion which was used in Chapter 3 had not been employed here. However, the results for the low Q_{ss1} value also show the current at low gate bias is larger than the saturation value with a high Q_{ss1}. The field pattern showed that the Si-sapph interface was depleted at low gate bias. This points out another difficulty with the depletion model which was

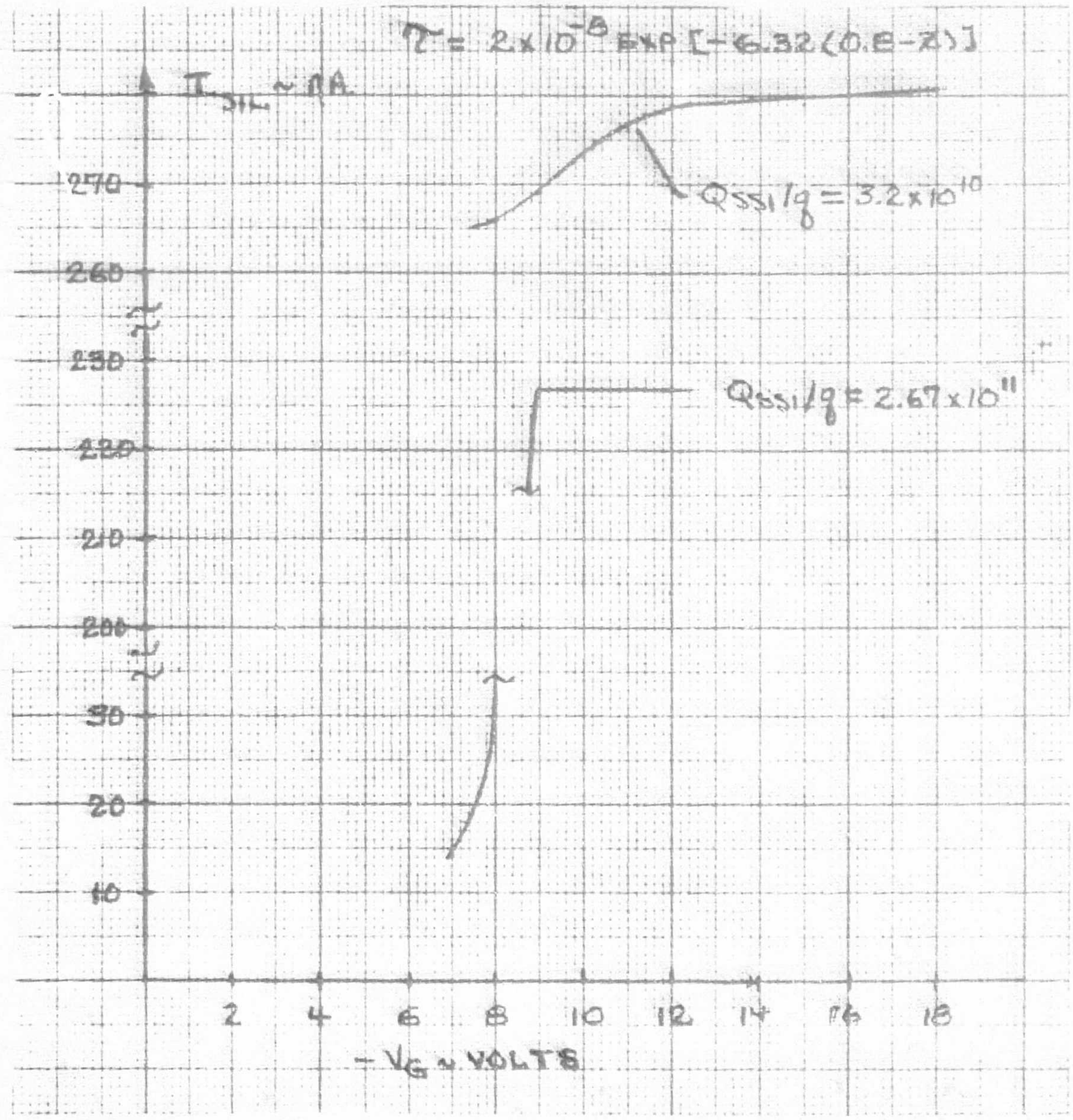

Figure 4.7 Junction Current vs. Gate Bias

anticipated in the previous section. Namely, this model assumes all current in the depletion region is collected; however, even if the si-sapph interface is depleted, at low gate bias the radial field component is so low that the generated carriers could not be collected before they recombine. Furthermore, most of the increased generation current for the smaller Q_{ss1} value represents holes which would be generated far removed from the P+ N junction thus making collection even more unlikely. Otherwise, the current vs. gate bias curves show that the current increase after through depletion (~ 7nA) observed by Kranzer is too large to be accounted for by extension of the depletion region further into the silicon not under the gate.

Finally, Figures 4.8 and 4.9 show the field distributions in the silicon after through depletion occurs. Values for the potential along the interface agree well enough with those obtained with the simplified model considering the differences in the parameters used. The results in Figure 4.8 are for $V_G = -18V$ which is before inversion sets in according to this model, while in Figure 4.9 $V_G = -24V$ and almost all of the $Si-SiO_2$ interface under the electrode is inverted. The results in Figure 4.9 agree qualitatively with what one expects to happen when inversion sets in. The radial component of the field in the top layer of the silicon film is reduced and the collection efficiency drops. This result can of course explain the fall off in the junction current after inversion begins.

4.6 Conclusions

The results obtained with the models discussed in this chapter show the following:

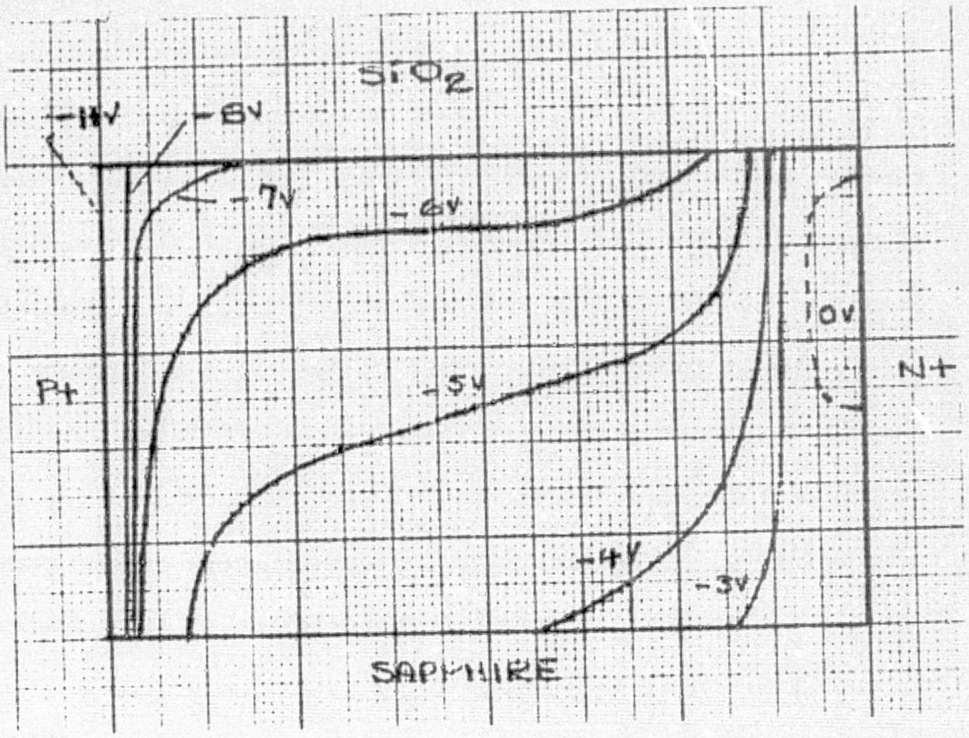

Figure 4.8 Field Pattern After Through-Depletion but Before Inversion $V_G = -18v$

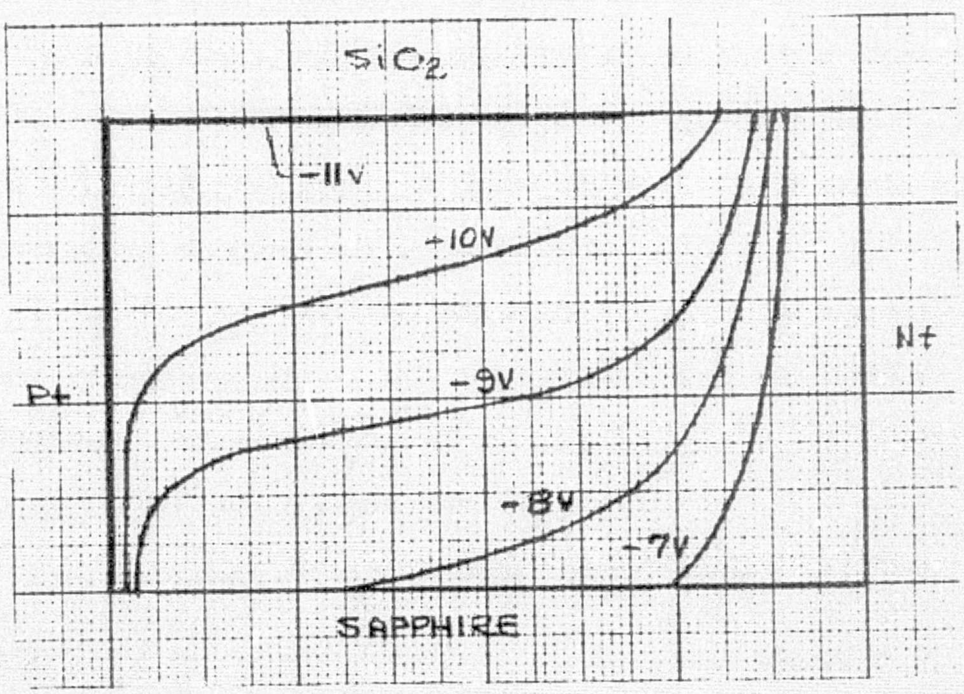

Figure 4.9 Field Pattern After Inversion begins. $V_G = -21V$

1. The actual charge distribution is probably significantly different from the depletion model. Consequently the depletion of carriers from the silicon-sapphire interface proceeds more slowly than predicted by the depletion model. There is a pile-up of holes at the Si-SiO_2 interface and of electrons at the Si-Sapph interface for an N-type film.
2. The depletion model predicts the advancement of a parallel depletion edge from the Si-SiO_2 interface; however, unless a fixed positively charged layer is assumed to exist at the Si-Sapph interface, a depletion occurs also from the bottom interface. The field strength in the bottom depletion region is low. Thus if such a region did in fact exist, thermally generated carriers in the region would not be collected. If one assumes that all the carriers are collected, the junction current calculated using an extrapolated lifetime profile is much in excess of the measured values. This latter difficulty is to some extent avoided by using a lifetime profile such as used in Chapter 3.
3. The field pattern obtained after through-depletion and before inversion shows that the collection efficiency of the structure should be significantly enhanced over that obtained before through depletion occurs.
4. The field pattern obtained after inversion at the Si-SiO_2 interface has begun shows that the collection efficiency should drop significantly with inversion.
5. The simulations gave current vs gate bias results grossly different from the measurements; however, they indicated that

the increase in the current with gate bias after through depletion is not simply the result of extension of the depletion layer into the region not under the gate electrode, although this phenomena is also involved (see Figure (4.8)).

Experience with the program operation led to the following conclusions:

6. The extended two-dimensional depletion model converges very slowly even though an attempt was made to minimize the number of points required to span the field of interest by using coarse, fine, and interpolating fields. Such a simulation model is expensive to implement for studying the effects of parameters on the C-V and 1-V curves. It is estimated that a simulation with adequate convergence would cost approximately $1 K at external computer time rates at MSU ($360/hr). Application of further programming and numerical analysis expertise could possibly reduce the cost.
7. The two-dimensional model including the continuity equations is even more expensive to implement. However, this model may very well be more useful in gaining insight into the physical phenomena. A disadvantage, other than the extensive amount of computing time, is that mobility parameters are needed, and the scattering phenomena itself is complex in the thin film. Perhaps for the reverse bias condition the scattering phenomena though important is still secondary.

The few results obtained here show that the very small lifetime near the Si-Sapph interface need not necessarily manifest itself in as large a current value as predicted by a depletion model. Very possibly, a region of net recombination may occur thus reducing the actual number of carriers collected.

CHAPTER 5

CONCLUSIONS

Concerning the capacitance vs. gate bias curves measured by Kranzer,[6] the following conclusions are made:

1. The initial decrease of the capacitance can be described well by a one-dimensional depletion model.
2. As the depletion extends to the silicon-sapphire interface, the majority carrier concentration there is expelled by increasing the gate bias. Three types of behavior are possible:
   (a) Abrupt expulsion and an abrupt drop in the C-V curve.
   (b) A gradual expulsion and gradual reduction of the C-V curve as observed by Kranzer.
   (c) A threshold may be observed, in some cases resulting in inversion at the Si-SiO_2 interface before depletion occurs.

   The behavior may be explained by the presence of a non-uniform fixed charge distribution on the silicon-sapphire interface and by the fact that the depletion occurs as a distributed field effect in which carrier diffusion, scattering, generation and recombination of carriers are involved.
3. The flat part of the C-V curve exhibits a minimum capacitance which is determined mainly by the capacitance of the sapphire, by the overlap capacitance, and by the parasitic in the measurement which cannot be made zero even with

careful guarding. The overlap and parasitic are dominant with 1 - 1.5 pF due to the sapphire.

4. The rise in the C-V curve with further increase in bias is due to inversion of the Si-SiO_2 interface region.

Concerning the junction current vs. gate bias curves measured by Kranzer,[6] the following conclusions are made:

5. The beginning part of the curve rises because of collection of carriers generated in a region which is continually expanded as the gate bias increases. This portion of the I-V curve is useful for obtaining an effective lifetime using a one-dimensional analysis.

6. Depletion through to the silicon-sapphire interface precedes more slowly than predicted by a one-dimensional model. However, it appears reasonable to treat the depletion as a surface phenomena with an increase in collected current due to a surface generation current as the depleted area grows. After depletion of the interface there is a small (12%) increase in current which may be attributed in part to the decrease of the radial transit time and the lateral increase (6%) of the depleted volume as the gate bias is increased further.

7. When inversion of the Si-SiO_2 interface occurs there is a substantial decrease in the radial field and an increase in the radial transit time, which should be accompanied by an increase in the electron concentration on the silicon-sapphire interface and in the hole concentration on the Si-SiO_2 interface. These increases in carrier densities

should result in a reduction in net generation; hence, the collected current drops as observed experimentally.

Concerning the utility of the Gate-Controlled-Diode for lifetime measurements, the following conclusions are made:

8. An "effective-lifetime" profile can be constructed from the C-V and I-V curves using the depletion model. This profile will be meaningful for data obtained for, probably, 50 - 75% of through-depletion and can be extrapolated to through-depletion.

9. The actual generation lifetime will be less than the "effective-lifetime." By obtaining the current at through-depletion and at saturation for a large junction bias voltage, the ratio of the former to the latter is obtained. The "effective lifetime" may by multiplied by this ratio to obtain a better estimate of the generation lifetime.

Concerning the utility of the simulation programs, the following conclusions are made:

10. The two-dimensional programs are too expensive to use for routine interpretation of data. The simplified two-dimensional program is useful for estimating the minimum capacitance and is economical.

11. The two-dimensional program including the continuity equations appears to be the most useful for obtaining insight into charge distributions and carrier flow, but it is very expensive to operate. Further refinements and operation of this program should be carried out.

12. A more extensive one-dimensional model may very well be useful in studying the falling part of the C-V curve. It would not be

predictive of current flow but would probably require input data from the current measurements. Nevertheless, more accurate modeling of charge distributions may be obtained using a model including the continuity equation. Such a model whould be inexpensive to implement.

REFERENCES

1. D. R. Collins, et. al., "Charge-Coupled Devices Fabricated Using Aluminum-Anodized Aluminum-Aluminum Double-Level Metallization," J. ELECTROCHEM. SOC.: SOLID STATE, Vol. 120, No. 4, pp. 521-526, April, 1973.

2. R. J. Krambeck, et. al., "Conductively Connected Charge-Coupled Device," IEEE TRANS. ELECT. DEVICES, Vol. ED -21, No. 1, pp. 70-72, Jan., 1974.

3. W. F. Kosonocky and J. E. Carnes., "Two-Phase Charge-Coupled Devices with Overlapping Polysilicon and Aluminum Gates," RCA Review, Vol., 34, pp. 164-203, Mar., 1973.

4. J. D. Gassaway, "Electrostatic Analysis of Charge-Coupled Structures," Interim Report, EIRS-EE-74-1, NAS 8-26749, January, 1974.

5. D. Kranzer, "Spatial Dependencies of the Carrier Lifetime in Thin Films of Silicon on Sapphire," APPL. PHYS. LETTERS, Vol. 25, No. 2, pp. 103-105, July 15, 1974.

6. D. Kranzer, Private Communication.

7. John E. Meyer, Jr., An Experimental Investigation of Low Level Phenomena in Silicon-on-Sapphire Devices, PhD Thesis, Rutgers University, May, 1972.

8. F.P. Heiman, "Thin Film Silicon-on-Sapphire Deep Depletion MOS Transistors", IEEE Trans. on Elect. Devices, Vol. ED-13, No.12, pp885-862, Dec. 1966.

9. F.P. Heiman,"Donor Surface States and Bulk Acceptor Traps in Silicon-on-Sapphire Films", Applied Phys. Lett.,Vol.11,No.4, pp132-134,Aug.1967.

10. J.F. Allison,D.J. Dumin,F.P. Heiman,C.W. Mueller, and P.H. Robinson, "Thin-Film Silicon:Preparation,Properties, and Device Applications", Proc. of IEEE, Vol.57,No.9,pp1490-1498, Sept.1969.

11. J.H. Scott and J.R. Burns,"Low Temperature Processing of CMOS In Integrated Circuits on Insulating Substrates", Electrochem. Soc. Meeting at Los Angeles, Abstract. No. 138, May10-15,1970.

APPENDIX A

SIMPLIFIED TWO DIMENSIONAL ANALYSIS

```
C
C     MAIN PROGRAM -- SIMPLIFIED ANALYSIS OF GCD
C     THIS IS THE SECOND MODIFIED PROGRAM.
C
      COMMON A(61),B(61),C(61),D(61),E(61),QSAP(61),W(61,61),DMAX,
     *CP(41),TAU(41)
      DIMENSION QB(41),DPSIX(41),GENR(41),X(61),PSIXO(20),MPUN(20),
     *QSS1(21),DA2(41),ALPHA(41),VTH2(41),PSISU(41)
      REAL NI,IREC
      NI=1.45E10
      EO=8.854E-14
      EPSI=11.7*EO
      EPSO=3.9*EO
      EPSAA=11.6*EO
      EPSAT=9.4*EO
      H=3.8E-2/60.
      PIA=3.1416*EPSAA/H
      PIB=3.1416*EPSAT*H
      Q=1.6E-19

      W1=1.524E-2
      W2=1.27E-2
      W3=W1
      CSAP=EPSAA/H
      CLAT=200.*H*EPSAT/W2**2
      READ(5,500) QSSP,QSSN,QSS2,S
  500 FORMAT(4E10.3)
      QSSP=Q*QSSP
      QSSN=Q*QSSN
      QSS2=Q*QSS2
      READ(5,504) TSIM,TOXM,MODE
  504 FORMAT(2F10.3,I10)
      DWA=8.E-5*(EXP(4.*TSIM)-1.0)
      WA=W1+1.905E-3+DWA
      WB=W2-1.905E-3-DWA
      A1=3.1416*((W1+1.905E-3)**2-W1**2)
      A2=3.1416*(WA**2-(WA-DWA)**2)
      A3=3.1416*((WA+WB)**2-WA**2)
      BETA=ALOG(QSSN/QSSP)/WB
      DO 1 I=1,21
    1 QSS1(I)=QSSP*EXP(BETA*(I-1)*WB/20.)
      CALL PARAM(TSIM)
      READ(5,506) VGLIM,DLIM,DVG,LIM
  506 FORMAT(3F10.3,I10)
      TSI=1.E-4*TSIM
      TOX=1.E-4*TOXM
C     COMPUTE THE FIELD COEFFICIENTS.
      DO 2 I=1,21
    2 X(I)=(I-1)*WA/20
      DO 4 I=22,41
    4 X(I)=WA+(I-21)*WB/20
      DO 6 I=42,61
    6 X(I)=W1+W2+(I-41)*W3/20.
      DO 8 I=2,60
      A(I)=PIA*(X(I+1)-X(I-1))*(X(I+1)+2.*X(I)+X(I-1))/4.
      B(I)=PIB*(X(I)+X(I-1))/(X(I)-X(I-1))
      D(I)=PIB*(X(I+1)+X(I))/(X(I)-X(I-1))
      E(I)=A(I)
    8 C(I)=A(I)+B(I)+D(I)+E(I)
C     COMPUTE THE DIFFERENTIAL AREA DA2(I)
      C2=0.
      ZO=3.*TOX
      Z1=0.
      RO=W1+1.905E-3
      R1=RO
      DO 9 I=1,40
      Z2=I*TSIM/40.
      R2=RO+8.E-5*(EXP(4.*Z2)-1.0)
      ZINV=1./(Z1+ZO)+1./(Z2+ZO)
      DA2(I)=3.1416*(R2-R1)*(R2+R1)
      C2=C2+DA2(I)*ZINV
      Z1=Z2
    9 R1=R2
      C2=1.5E16*EPSO*C2
```

ORIGINAL PAGE IS OF POOR QUALITY

```
C         F1 CONTAINS THE AVERAGE FACTOR 0.5  AND DY.
C         F2 CONTAINS .5 FOR AVERAGE,DY,AND EPSI
      F1=0.5*Q*TSI/40.
      F2=0.5*(TSI/40.)/EPSI
      DO 10 J=2,41
      QB(J)=QB(J-1)+F1*(CB(J)+CB(J-1))
      DPSIX(J)=DPSIX(J-1)+F2*(QB(J)+QB(J-1))
   10 GENR(J)=GENR(J-1)+0.25*NI*(TSI/40.)*(1./TAU(J)+1./TAU(J-1))
C         CALCULATE INITIAL CAPACITANCES.
      COX=EPSO/TOX
      C1=1.E12*A1*COX
      C3=1.E12*A3*COX
      CGM=C1+C2+C3+1.
      WRITE(6,600) CGM,TOXM,TSIM
  600 FORMAT(//,10X,'CGM,PF=',F8.3,5X,'TOX,M=',F5.3,5X,'TSI,M=',F5.3//
     *13X,'C3 ',12X,'CGPF',12X,'CN',12X,'IREC',12X,'VG',13X,'YD',13X,
     *'QEL',//)
      READ(5,508) VJ
  508 FORMAT(F10.3)
C         CALCULATE C-V,I-V CURVES BEFORE THROUGH DEPLETION.
      Q2=0.
      DO 12 J=2,41
      XD=(J-1)*TSI/40.
      YD=1.E4*XD
      CSI=EPSI/XD
      CSER=CSI*COX/(COX+CSI)
      C3=1.E12*A3*CSER
      CG=C1+C2+C3+1.
      CN=CG/CGM
      DQ=-QSS2-QB(J)
      VQ=QSS2/CSI+DPSIX(J)
      VG=DQ/CSER+VQ
      IREC=1.E9*(A2+A3)*Q*GENR(J)
      ALPHA(J)=1.-CSER/COX
      VTH2(J)=CSER*VQ/COX
      Q1=A1*COX*(VG-VJ-1.1)
      Q2=Q2+COX*(VG-(VTH2(J)+VTH2(J-1))/2.)*DA2(J)
      Q3=A3*DQ
      QEL=Q1+Q2+Q3
   12 WRITE(6,602) C3,CG,CN,IREC,VG,YD,QEL
  602 FORMAT(10X,F10.3,5X,F10.3,5X,F10.3,5X,F10.3,5X,F10.3,5X,F10.3,
     *5X,F10.3)
      DPSI=DPSIX(41)
      QSUB=QB(41)
C         THE PRESENT VALUES OF CSI,CSER,COX ARE THE VALUES
C         NEEDED FOR LATER CALCULATIONS
C         SOLVE THE INITIAL FIELD IN THE SAPPHIRE
      VINV=VJ+.55
      DO 14 I=1,21
   14 W(I,61)=VJ+1.1
      LOOP=0
      OMEGA=1.8
   16 DMAX=0.0
      CALL RELAX(OMEGA)
      LOOP=LOOP+1
      IF(DMAX.GT.DLIM) GO TO 16
      DO 18 I=1,61
   18 QSAP(I)=CSAP*(W(I,61)-W(I,60))
      WRITE(6,604) LOOP
      CALL OUTPU
      IF(MODE.EQ.0) GO TO 1600
      VGMIN=-(QSS1(2)-QSAP(22)+(1.-CSER/CSI)*QSS2+QSUB)/CSER+DPSI
      VGMAX=-(QSS1(20)-QSAP(40)+(1.-CSER/CSI)*QSS2+QSUB)/CSER+DPSI
      WRITE(6,606) VGMIN,VGMAX
  606 FORMAT(/,20X,'VGMIN=',F10.3,5X,'VGMAX=',F10.3/)
C         START SOLUTION FOR PUNCHTHROUGH CONDITION.
      VG=VGMIN
      VG=-16.0
 1000 CONTINUE
      ITER=0
      MFLAG=0
   40 LOOP=0
      MNEW=0
      ILO=22+MFLAG
      DO 42 I=ILO,40
      M=I-21
      VTH=(QSAP(I)-QSUB-QSS1(M+1))/CSER-QSS2/COX+DPST
      IF(VG.LT.VTH) MPUN(M)=1
   42 IF(MPUN(M).EQ.1.AND.MPUN(M+1).EQ.0) MNEW=M
```

```
      MFLAG= MNEW
C        SET B.C. AND CARRY OUT THE RELAXATION.
800   LOOP=LOOP+1
      ITER=ITER+1
      DMAX=0.
      DO 70 I=22,40
      WOLD=W(I,61)
      M=I-21
      IF(MPUN(M).EQ.1) GO TO 66
      W(I,61)=0.
      PSIXO(M)=(COX*VG+QSS2+CSI*DPSI)/(COX+CSI)
      GO TO 68
66    PSIXO(M)=VG+(QSS1(M+1)+QSUB+QSS2-QSAP(I))/COX
      IF(PSIXO(M).LT.VINV) PSIXO(M)=VINV
      W(I,61)=(CSI*(PSIXO(M)-DPSI)+CSAP*W(I,60)+2.*CLAT*(W(I-1,61)
     *+W(I+1,61))+QSS1(M+1)+QSUB)/(CSI+CSAP+2.*CLAT)
      IF(W(I,61).GT.0.0) W(I,61)=0.0
68    DW=ABS(W(I,61)-WOLD)
      IF(DW.GT.DMAX) DMAX=DW
70    CONTINUE
75    CALL RELAX(OMEGA)
      DO 82 I=2,60
82    QSAP(I)=CSAP*(W(I,61)-W(I,60))+CLAT*(2.*W(I,61)-W(I-1,61)
     *-W(I+1,61))
      IF(DMAX.LT.DLIM) GO TO 100
      GO TO 800
100   CALL OUTPU
      WRITE(6,604) ITER
C        CALCULATE Q AND IREC
      QOLD=QEL
      QEL=0.
C        CALCULATE Q1
      Q1=COX*A1*(VG-VJ-1.1)
C        CALCULATE Q2
      Q2=0.
      DO 150 J=2,41
      PSISU(J)=ALPHA(J)*(VG-VJ-1.1)+VTH2(J)
      IF(PSISU(J).LT.VINV) PSISU(J)=VINV
150   Q2=Q2+DA2(J-1)*COX*(VG-(PSISU(J)+PSISU(J-1))/2.)
C        CALCULATE Q3
      Q3=0.
      CUR=IREC
      DO 108 M=1,19
      I=21+M
      DQEL=(3.1416*A(I)/PIA)*COX*(VG-PSIXO(M))
      CUR=CUR+3.1416E9*Q*NI*S*A(I)*MPUN(M)/PIA
108   Q3=Q3+DQEL
      Q3=Q3+1.507*A(21)/PIA*COX*(VG-VJ-1.1)+1.507*A(41)/PIA*COX*VG
      QEL=Q1+Q2+Q3
      CG=1.E12*(QOLD-QEL)/DVG+1.
      CN=CG/COM
      WRITE(6,620) QEL,CG,CN,VG,CUR
620   FORMAT(/,20X,'QEL=',F11.5,5X,'CG,PF=',F7.3,5X,'CN=',F6.3,5X,'VG=',
     *F7.3,5X,'IREC=',F7.3/)
604   FORMAT(/,20X,'ITER OR LOOP=',I4/)
110   VG=VG-DVG
      DMAX=1.
      IF(VG.GE.VGLIM) GO TO 1000
1600  STOP
      END
```

```
      SUBROUTINE PARAM(TSIM)
      COMMON A(61),B(61),C(61),D(61),F(61),QSAP(61),W(61,61),DMAX,
     *CU(41),TAU(41)
      DO 24 I=1,41
      X=(I-1)*TSIM/40.
      IF(X.GE.0..AND.X.LT.0.1) GO TO 2
      IF(X.GE.0.1.AND.X.LT.0.2) GO TO 4
      IF(X.GE.0.2.AND.X.LT.0.3) GO TO 6
      IF(X.GE.0.3.AND.X.LT.0.4) GO TO 8
      IF(X.GE.0.4.AND.X.LT.0.5) GO TO 10
      IF(X.GE.0.5.AND.X.LT.0.6) GO TO 12
      IF(X.GE.0.6.AND.X.LT.0.7) GO TO 14
      IF(X.GE.0.7) GO TO 16
2     Z=0.0
      G=9.1E15
      F=6.52
      GO TO 18
4     Z=0.1
      G=4.95E15
      F=5.52
      GO TO 18
6     Z=0.2
      G=2.65E15
      F=4.45
      GO TO 18
8     Z=0.3
      G=1.63E15
      F=3.56
      GO TO 18
10    Z=0.4
      G=1.28E15
      F=2.97
      GO TO 18
12    Z=0.5
      G=9.5E14
      F=2.36
      GO TO 20
14    Z=0.6
      G=7.5E14
      F=2.07
      GO TO 20
16    Z=0.7
      G=6.1E14
      F=2.07
      GO TO 20
18    TAU(I)=4.6E-8/EXP(2.08*X)
      GO TO 22
20    TAU(I)=1.7E-8
22    CU(I)=G/EXP(F*(X-Z))
24    CONTINUE
      RETURN
```

ORIGINAL PAGE IS
OF POOR QUALITY

```
      SUBROUTINE OUTPU
      COMMON A(61),B(61),C(61),D(61),E(61),QSAP(61),W(61,61),DMAX,
     *CB(41),TAU(41)
      WRITE(6,100)
100   FORMAT(/20X,'SAPPHIRE INTERFACE FIELD,COUL.CM**2'/)
      WRITE(6,102) (QSAP(I),I=2,21,2)
      WRITE(6,102) (QSAP(I),I=22,41,2)
      WRITE(6,102) (QSAP(I),I=42,61,2)
102   FORMAT(10E11.4)
      WRITE(6,104)
104   FORMAT(/,20X,'SAPPHIRE POTENTIAL FIELD'/)
      DO 2 M=1,61,3
      J=62-M
 2    WRITE(6,106) (W(I,J),I=2,21,2)
      WRITE(6,108)
      DO 4 M=1,61,3
      J=62-M
 4    WRITE(6,106) (W(I,J),I=22,41,2)
      WRITE(6,108)
      DO 6 M=1,61,3
      J=62-M
 6    WRITE(6,106) (W(I,J),I=42,61,2)
106   FORMAT(10F10.3)
108   FORMAT(/)
      RETURN
      END
```

```
      SUBROUTINE RELAX(OMEGA)
      COMMON A(61),B(61),C(61),D(61),E(61),QSAP(61),W(61,61),DMAX,
     *CB(41),TAU(41)
      DO 4 J=2,60
      DO 2 I=2,60
      WOLD=W(I,J)
      WTIL=(A(I)*W(I,J-1)+B(I)*W(I-1,J)+D(I)*W(I+1,J)+E(I)*W(I,J+1))
     */C(I)
      W(I,J)=(1.-OMEGA)*WOLD+OMEGA*WTIL
      DW=ABS(W(I,J)-WOLD)
 2    IF(DW.GT.DMAX) DMAX=DW
      W(1,J)=W(2,J)
      W(61,J)=W(60,J)
 4    CONTINUE
      DO 6 I=1,61
    6 W(I,1)=0.0
      RETURN
      END
```

ORIGINAL PAGE IS
OF POOR QUALITY

APPENDIX B

TWO DIMENSIONAL ANALYSIS INCLUDING THE CONTINUITY EQUATIONS

```
DIMENSION W(25,11),V(41,11),U(93,56),UA(13,7),QS(93,56)
DIMENSION AAR(26),BAR(26),DAR(26),EAR(26)
DIMENSION AAZ(12),BAZ(12),DAZ(12),EAZ(12)
DIMENSION ABR(42),BBR(42),DBR(42),EBR(42)
DIMENSION ABZ(12),BBZ(12),DBZ(12),EBZ(12)
DIMENSION ACR(94),BCR(94),DCR(94),ECR(94)
DIMENSION ACZ(61),BCZ(61),DCZ(61),ECZ(61)
DIMENSION X(100),CS(51),PHI(51),TAU(51),ZB(12)
DIMENSION P(93,51),Q(93,51),G(93,51)
REAL NI,ND,NI2
DP=5.2
PD=1./DP
DN=15.
ND=1./DN
NI=1.5E10
NI2=NI**2
NWRIT=0
QSS1=0.
QSS2=2.67E11
LTOP=50
Q=1.6E-19
QSS1=QSS1*Q
QSS2=QSS2*Q
VT=0.0259
TEE=0.6
TOX=0.4
TSI=0.6
CSS=6.E15
TAU0=2.E-6
BETA1=3.92
BETA2=6.32
PI=3.1416
EPSA=12.3*8.854E-14
EPSB=11.7*8.854E-14
EPSC=3.7*8.854E-14
EPS0=8.854E-14
I1=9
I2=17
I3=25
L1=8
L2=8
L3=8
K1=10
J1=11
W1=140.
W2=152.
W3=140.
L4=8
I4=9
L5=32
I5=41
K2=10
J2=11
L6=32
I6=33
L7=92
I7=93
I8=82
K3=50
J3=51
K4=55
J4=56
K5=60
J5=61
H=TSI/(J3-3)
RH=1./H
HS1=100.*H
HS2=100.*H
```

```
      TW=0.5/VT
      TAUP=1.E-6
      TAUN=1.E-6
C     COMPUTE COEFFICIENTS IN U-FIELD
      DO 2 I=1,I1
    2 X(I)=(I-1)*W1/L1
      DO 4 I=I1,I2
    4 X(I)=W1+(I-I1)*W2/L2
      DO 6 I=I2,I3
    6 X(I)=W1+W2+(I-I2)*W3/L3
      IU=I3-1
      DO 8 I=2,IU
      AAR(I)=PI*X(I)*(X(I+1)-X(I-1))
      BAR(I)=PI*(X(I)+X(I-1))/(X(I)-X(I-1))
      CAR(I)=PI*(X(I+1)+X(I))/(X(I+1)-X(I))
    8 DAR(I)=PI*X(I)*(X(I+1)-X(I))
      ALPHA=2.
      DO 10 J=1,J1
   10 Y(I)=-TSI*(ALPHA**(J1-J)-1.)/(ALPHA-1.)
      DO 12 J=2,K1
      AAZ(J)=EPSA/(X(J)-X(J-1))
      BAZ(J)=EPSA*(X(J+1)-X(J))/2.
      CAZ(J)=BAZ(J)
   12 DAZ(J)=EPSA/(X(J+1)-X(J))
C     CALCULATE COEFFICIENTS FOR V-FIELD.
      DO 14 I=1,I4
   14 X(I)=(I-1)*W1/(4.*L4)+3.*W1/4.
      DO 16 I=I4,I5
   16 X(I)=(I-I4)*W2/L5+W1
      IU=I5-1
      DO 18 I=2,IU
      ABR(I)=PI*X(I)*(X(I+1)-X(I-1))
      BBR(I)=PI*(X(I)+X(I-1))/(X(I)-X(I-1))
      CBR(I)=PI*(X(I+1)+X(I))/(X(I)-X(I-1))
   18 DBR(I)=ABR(I)
      K2=J3-3
      ALPHA=1.25
   20 AN=(ALPHA**K2-1.-KA*(ALPHA-1.))*(ALPHA-1.)
      AD=(K2-1)*ALPHA**K2-K2*ALPHA**(K2-1)+1.
      DA=-AN/AD
      ALPHA=ALPHA+DA
      RATIO=ABS(DA/ALPHA)
      IF(RATIO.GT.0.01) GO TO 20
      HO=TSI/(J3-3)
      DO 22 J=1,J2
   22 ZB(J)=-HO*(ALPHA**(J2-J)-1.)/(ALPHA-1.)
      DO 24 J=2,K2
      ABZ(J)=EPSA/(ZB(J)-ZB(J-1))
      BBZ(J)=EPSA*(ZB(J+1)-ZB(J-1))/2.
      CBZ(J)=BBZ(J)
   24 DBZ(J)=EPSA/(ZB(J+1)-ZB(J))
C     COEFFICIENTS FOR U-FIELD.
      DO 26 I=1,I6
   26 X(I)=(I-1)*W2/(2.*L2*L6)+W1
      DO 28 I=I6,I7
   28 X(I)=X(I6)+(I-I6)*W2/(2.*L5)
      IU=I7-1
      DO 30 I=2,IU
      ACR(I)=PI*X(I)*(X(I+1)-X(I-1))
      BCR(I)=PI*(X(I)+X(I-1))/(X(I)-X(I-1))
      CCR(I)=PI*(X(I+1)+X(I))/(X(I+1)-X(I))
   30 DCR(I)=ACR(I)
      X(1)=ZB(J2-2)
      X(2)=ZB(J2-1)
      X(3)=0.
      DO 32 J=4,J3
   32 X(J)=TSI*(J-3)/(J3-3)
      DO 34 J=J3,J4
   34 X(J)=X(J3)+TOX*(J-J3)/(J4-J3)
      DO 36 J=J4,J5
   36 X(J)=X(J4)+TEL*(J-J4)/(J5-J4)
      ACZ(2)=EPSA/(X(2)-X(1))
      BCZ(2)=EPSA*(X(3)-X(1))/2.
      CCZ(2)=BCZ(2)
      DCZ(2)=EPSA/(X(3)-X(2))
      ACZ(3)=EPSA/(X(3)-X(2))
      BCZ(3)=(EPSO*(X(4)-X(3))+EPSA*(X(3)-X(2)))/2.
      CCZ(3)=BCZ(3)
      DCZ(3)=EPSO/(X(4)-X(3))
```

```
      DO 38 J=4,K3
      ACZ(J)=EPSB/(X(J)-X(J-1))
      BCZ(J)=EPSB*(X(J+1)-X(J-1))/2.
      DCZ(J)=BCZ(J)
   38 ECZ(J)=EPSB/(X(J+1)-X(J))
      ACZ(J3)=EPSB/(X(J3)-X(J3-1))
      BCZ(J3)=(EPSC*(X(J3+1)-X(J3))+EPSB*(X(J3)-X(J3-1)))/2.
      DCZ(J3)=BCZ(J3)
      ECZ(J3)=EPSC/(X(J3+1)-X(J3))
      JU=J4-1
      JL=J3+1
C     DO THE OXIDE REGION.
      DO 40 J=JL,JU
      ACZ(J)=EPSC/(X(J)-X(J-1))
      BCZ(J)=EPSC*(X(J+1)-X(J))/2.
      DCZ(J)=BCZ(J)
   40 ECZ(J)=EPSC/(X(J+1)-X(J))
      ACZ(J4)=EPSC/(X(J4)-X(J4-1))
      BCZ(J4)=(EPSO*(X(J4+1)-X(J4))+EPSC*(X(J4)-X(J4-1)))/2.
      DCZ(J4)=BCZ(J4)
      ECZ(J4)=EPSO/(X(J4+1)-X(J4))
      JL=J4+1
      JU=J5-1
      DO 42 J=JL,JU
      ACZ(J)=EPSO/(X(J)-X(4-1))
      BCZ(J)=EPSO*(X(J+1)-X(J))/2.
      DCZ(J)=BCZ(J)
   42 ECZ(J)=EPSO/(X(J+1)-X(J))
      DO 43 J=3,J3
      CS(J)=CSS*EXP(-BETA1*(TSI-X(J)))
      TAU(J)=TAUO*EXP(-BETA2*(TSI-X(J)))
   43 PHI(J)=VT*BETA1*X(J)
      DO 708 J=3,J3
      DO 708 I=2,I7
      P(I,J)=CS(J)
      N(I,J)=NI**2/CS(J)
  708 CONTINUE
  800 READ(5,802) VJ,VG,WRIT
  802 FORMAT(3F10.3)
      IF(VJ.GT.0) STOP
      MWRIT=0
      VJ=VJ-1.1
      IF(WRIT.GT.1.0) MWRIT=1
C     SET ALL FIXED BOUNDARY VALUES.
      DO 44 I=1,I1
   44 V(I,J1)=VJ
      DO 45 I=1,I4
   45 V(I,J2)=VJ
      DO 46 I=I2,I3
   46 V(I,J1)=0.
      DO 48 J=3,J3
      V(1,J)=VJ
   48 V(I7,J)=PHI(J)
      DO 50 J=J3,J4
      V(1,J)=VJ+(J-J3)*(VG-VJ)/(J4-J3)
   50 V(I7,J)=PHI(J3)
      DO 52 I=1,I9
   52 V(I,J4)=VG
      IU=1+I7-I8
      DO 54 J=1,6
      VA(1,J)=VG
   54 VA(IU,J)=PHI(J3)
      DO 56 I=1,IU
   56 VA(I,6)=VG-(I-1)*(VG-PHI(J3))/(I7-I8)
C     START IN V-FIELD WITH RELAXATION.
      IPASS=0
      ICMAX=0
 1000 CONTINUE
      IPASS=IPASS+1
      IA=I1+1
      IB=I2-1
      DO 62 I=IA,I9
      IP=4+I-3*I1
   62 V(I,J1)=V(IP,J2)
      OMEGA=1.7
      DIJ=0.
      LOOP=1
      JLO=J1-2
      JHI=J1-1
```

ORIGINAL PAGE IS
OF POOR QUALITY

```
      IUP=I3-1
   64 JLO=JLO-1
      IF(JLO.LT.2) JLO=2
      RES=0.
      DO 68 J=JLO,JM1
      DO 66 I=2,IUP
      WOLD=W(I,J)
      A=AAW(I)*AAZ(J)
      B=BAW(I)*BAZ(J)
      D=DAW(I)*DAZ(J)
      F=EAW(I)*EAZ(J)
      C=A+B+D+F
      WTIL=(A*W(I,J-1)+B*W(I-1,J)+D*W(I+1,J)+F*W(I,J+1))/C
      W(I,J)=(1.-OMEGA)*WOLD+OMEGA*WTIL
      DW=W(I,J)-WOLD
      RES=RES+DW**2
   66 CONTINUE
      W(1,J)=W(2,J)
      W(I3,J)=W(IUP,J)
   68 CONTINUE
      DO 70 I=1,I3
      W(I,J)=W(I,2)
   70 CONTINUE
      LOOP=LOOP+1
      IF(LOOP.LE.10) GO TO 64
      IF(MWRIT.EQ.0) GO TO 77
      RMS=SQRT(RES)
      WRITE(6,500)
  500 FORMAT (/,20X,'DATA FOR W(I,J) FIELDS',/)
      WRITE(6,502) RMS
  502 FORMAT(/,20X,'RMS=',F6.3,/)
      WRITE(6,504)
  504 FORMAT(/,20X,'W(I,J) IN 3 ADJACENT FIELDS'/)
      DO 72 M=1,J1
      J=J1+1-M
      WRITE(6,506) (W(I,J),I=1,I1)
   72 CONTINUE
      WRITE(6,507)
  507 FORMAT(//,20X,'NEXT FIELD',//)
      DO 74  M=1,J1
      J=J1+1-M
      WRITE(6,506) (W(I,J),I=I1,I2)
   74 CONTINUE
      WRITE(6,507)
      DO 76 M=1,J1
      J=J1+1-M
      WRITE(6,506) (W(I,J),I=I2,I3)
   76 CONTINUE
      WRITE(6,507)
  506 FORMAT(10X,9F10.3)
   77 CONTINUE
C     DO THE V-FIELD.
C     LOCATE BOUNDARY VALUES IN W AND U FIELDS AND INTERPOLATE.
      IW=1+3*L1/4
      IR=I2-1
      DO 78 I=IW,IR
      VLO=W(I,K1)
      VHI=W(I+1,K1)
      K=4*(I-IW)+1
      V(K,1)=VLO
      V(K+1,1)=VLO+(VHI-VLO)/4.
      V(K+2,1)=VLO+(VHI-VLO)/2.
      V(K+3,1)=VLO+3.*(VHI-VLO)/4.
      V(K+4,1)=VHI
   78 CONTINUE
      DO 82 J=2,J2
      S=(ZB(J)-ZB(1))/ZB(1)
      V(1,J)=W(I1,K1)-S*(W(I1,J1)-W(I1,K1))
      V(I5,J)=W(I2,K1)-S*(W(I2,J1)-W(I2,K1))
   82 CONTINUE
      IF(IPASS.GT.1) GO TO 85
      V(I4+1,J2)=U(17,3)
      ILO=I4+2
      DO 84 I=ILO,I5
      M=33+2*(I-ILO)
      V(I,J2)=U(M,3)
   84 CONTINUE
   85 CONTINUE
C     RELAX THE V-FIELD.
```

```
      OMEGA=1.7
      LOOP=1
      IUP=I5-1
      JLO=J2-2
      JHI=J2-1
   86 JLO=JLO-1
      IF(JLO.LT.2)JLO=2
      RES=0.
      DO 90 J=JLO,JHI
      DO 88 I=2,IUP
      A=ABR(I)*ABZ(J)
      B=BBR(I)*BBZ(J)
      D=DBR(I)*DBZ(J)
      E=EBR(I)*EBZ(J)
      C=A+B+D+E
      VOLD=V(I,J)
      VTIL=(A*V(I,J-1)+B*V(I-1,J)+D*V(I+1,J)+E*V(I,J+1))/C
      V(I,J)=(1.-OMEGA)*VOLD+OMEGA*VTIL
      DV=V(I,J)-VOLD
      RES=RES+DV**2
   88 CONTINUE
   90 CONTINUE
      LOOP=LOOP+1
      IF(LOOP.LE.50) GO TO 86
      IF(JWRIT.EQ.0) GO TO 95
      WRITE(6,508)
  508 FORMAT(/,20X,'DATA FOR V(I,J) FIELD'/)
      RMS=SQRT(RES)
      WRITE(6,502) RMS
      WRITE(6,510)
  510 FORMAT(/,20X,'V(I,J) IN 2 ADJACENT FIELDS'/)
      DO 92 M=1,J2
      J=J2-M+1
      WRITE(6,512) (V(I,J),I=1,21,2)
   92 CONTINUE
      WRITE(6,507)
      DO 94 M=1,J2
      J=J2-M+1
      WRITE(6,512) (V(I,J),I=21,41,2)
   94 CONTINUE
  512 FORMAT(10X,11F8.2)
   95 CONTINUE
C     DO THE RELAXATION FOR THE U-FIELD
C     LOAD BOUNDARY VALUES FROM THE V-FIELD AND INTERPOLATE.
      U(1,1)=V(I4,J2-2)
      U(1,2)=V(I4,J2-1)
      U(I7,1)=V(I5,J2-2)
      U(I7,2)=V(I5,J2-1)
      U(I7,1)=V(I4+1,J2-2)
      DO96  I=I6,I7,2
      M=I4+2+(I-I6)/2
      U(I,1)=V(M,J1-2)
   96 CONTINUE
      DO 98 I=2,16
      U(I,1)=U(1,1)+(I-1)*(U(17,1)-U(1,1))/16
   98 CONTINUE
      DO 100 I=18,32
      U(I,1)=U(17,1)+(I-17)*(U(33,1)-U(17,1))/16
  100 CONTINUE
      IUP=I7-1
      DO 102 I=34,IUP,2
      U(I,1)=(U(I-1,1)+U(I+1,1))/2.
  102 CONTINUE
      RES=0.0
      LOOP=1
      OMEGA=1.7
  104 CONTINUE
C   ***************************************************************
      ICMAX=ICMAX+1
      CMAX=ICMAX*CSS
      RMS=0.
      QMS=0.
C        CALCULATE THE LATEST GENERATION RATE.
      J=3
      DO 106 I=2,IUP
  106 G(I,J)=1.E-3*ACR(I)*HS1*(NI2-P(I,J)*Q(I,J))
     */(TAU(J)*(P(I,J)+Q(I,J)+2.*NI))
      DO 107 J=4,K3
      DO 107 I=2,IUP
```

ORIGINAL PAGE IS
OF POOR QUALITY

```
 107   G(I,J)=1.E-P*ACR(I)*H*(NI2-P(I,J)*O(I,J))/
      *(TAU(J)*(P(I,J)+O(I,J)+2.*NI))
       J=J3
       DO 108 I=2,IUP
       G(I,J)=1.E-8*ACR(I)*HS2*(NI2-P(I,J)*O(I,J))/
      *(TAU(J)*(P(I,J)+O(I,J)+2.*NI))
 108   CONTINUE
C         THE NEXT 3 LOOPS CALCULATE THE CARRIER CONCENTRATIONS.
       OMEGA=0.5
       J=3
       IUP=I7-1
       DO 700 I=2,IUP
       A=ACR(I)*KH
       B=BCR(I)*H
       D=DCR(I)*H
       E=ECR(I)*KH
       AP=A*(1.-TV*(U(I,J)-U(I,J-1)))
       AO=A*(1.+TV*(U(I,J)-U(I,J-1)))
       BP=B*(1.-TV*(U(I,J)-U(I-1,J)))
       BO=B*(1.+TV*(U(I,J)-U(I-1,J)))
       DP=D*(1.-TV*(U(I,J)-U(I+1,J)))
       DO=D*(1.+TV*(U(I,J)-U(I+1,J)))
       EP=E*(1.-TV*(U(I,J)-U(I,J+1)))
       EO=E*(1.+TV*(U(I,J)-U(I,J+1)))
       CP=AO+BO+DO+EO
       CN=AP+BP+DP+EP
       CP=CP-AO
       CN=CN-AP
       POLD=P(I,J)
       OLD=O(I,J)
       IF(I.EQ.IUP) GO TO 670
       PTIL=(BP*P(I-1,J)+DP*P(I+1,J)+EP*P(I,J+1)+PD*G(I,J))/CP
       IF(I.EQ.2) GO TO 672
       OTIL=(BO*O(I-1,J)+DO*O(I+1,J)+EO*O(I,J+1)+ND*G(I,J))/CN
       GO TO 674
 670   CP=CP-DO
       PTIL=(BP*P(I-1,J)+EP*P(I,J+1)+PD*G(I,J))/CP
       P(I+1,J)=DO*P(I,J)/DP
       OTIL=(BO*O(I-1,J)+DO*O(I+1,J)+EO*O(I,J+1)+ND*G(I,J))/CN
       GO TO 674
 672   CN=CN-BP
       OTIL=(DO*O(I+1,J)+EO*O(I,J+1)+ND*G(I,J))/CN
       O(I-1,J)=BP*O(I,J)/BO
 674   CONTINUE
       P(I,J)=(1.-OMEGA)*POLD+OMEGA*PTIL
       O(I,J)=(1.-OMEGA)*OLD+OMEGA*OTIL
       IF(P(I,J).LT.0.) P(I,J)=0.
       IF(O(I,J).LT.0.) O(I,J)=0.
       IF(O(I,J).GT.CMAX) O(I,J)=CMAX
       IF(P(I,J).GT.CMAX) P(I,J)=CMAX
 700   CONTINUE
       DO 704 J=4,K3
       DO 702 I=2,IUP
       A=ACR(I)*KH
       B=BCR(I)*H
       D=DCR(I)*H
       E=ECR(I)*KH
       AP=A*(1.-TV*(U(I,J)-U(I,J-1)))
       AO=A*(1.+TV*(U(I,J)-U(I,J-1)))
       BP=B*(1.-TV*(U(I,J)-U(I-1,J)))
       BO=B*(1.+TV*(U(I,J)-U(I-1,J)))
       DP=D*(1.-TV*(U(I,J)-U(I+1,J)))
       DO=D*(1.+TV*(U(I,J)-U(I+1,J)))
       EP=E*(1.-TV*(U(I,J)-U(I,J+1)))
       EO=E*(1.+TV*(U(I,J)-U(I,J+1)))
       CP=AO+BO+DO+EO
       CN=AP+BP+DP+EP
       POLD=P(I,J)
       OLD=O(I,J)
       IF(I.EQ.IUP) GO TO 680
       PTIL=(AP*P(I,J-1)+BP*P(I-1,J)+DP*P(I+1,J)+EP*P(I,J+1)+PD*G(I,J))/
      *CP
       IF(I.EQ.2) GO TO 682
       OTIL=(AO*O(I,J-1)+BO*O(I-1,J)+DO*O(I+1,J)+EO*O(I,J+1)+ND*G(I,J))/
      *CN
       GO TO 684
 680   CP=CP-DO
       PTIL=(AP*P(I,J-1)+BP*P(I-1,J)+EP*P(I,J+1)+G(I,J))/CP
       P(I+1,J)=DO*P(I,J)/DP
```

```
      OTIL=(AO*O(I,J-1)+BO*O(I-1,J)+DO*O(I+1,J)+EO*O(I,J+1)+ND*G(I,J))/
     *CN
      GO TO 684
 682  CN=CN-BP
      OTIL=(AO*O(I,J-1)+DO*O(I+1,J)+EO*O(I,J+1)+ND*G(I,J))/CN
      O(I-1,J)=BP*O(I,J)/BO
 684  CONTINUE
      P(I,J)=(1.-OMEGA)*POLD+OMEGA*PTIL
      IF(P(I,J).LT.0.) P(I,J)=0.
      O(I,J)=(1.-OMEGA)*OLD+OMEGA*OTIL
      IF(O(I,J).LT.0.) O(I,J)=0.
      IF(O(I,J).GT.CMAX) O(I,J)=CMAX
      IF(P(I,J).GT.CMAX) P(I,J)=CMAX
 702  CONTINUE
 704  CONTINUE
      J=J3
      DO 706 I=2,IUP
      A=ACR(I)*RH
      B=BCR(I)*H
      D=DCR(I)*H
      E=ECR(I)*RH
      AP=A*(1.-TV*(U(I,J)-U(I,J-1)))
      AO=A*(1.+TV*(U(I,J)-U(I,J-1)))
      BP=B*(1.-TV*(U(I,J)-U(I-1,J)))
      BO=B*(1.+TV*(U(I,J)-U(I-1,J)))
      DP=D*(1.-TV*(U(I,J)-U(I+1,J)))
      DO=D*(1.+TV*(U(I,J)-U(I+1,J)))
      EP=E*(1.-TV*(U(I,J)-U(I,J+1)))
      EO=E*(1.+TV*(U(I,J)-U(I,J+1)))
      CP=AO+BO+DO+EO
      CN=AP+BP+DP+EP
      CP=CP-EO
      CN=CN-EP
      POLD=P(I,J)
      OLD=O(I,J)
      IF(I.EQ.IUP) GO TO 690
      PTIL=(AP*P(I,J-1)+BP*P(I-1,J)+DP*P(I+1,J)+PD*G(I,J))/CP
      IF(I.EQ.2) GO TO 692
      OTIL=(AO*O(I,J-1)+BO*O(I-1,J)+DO*O(I+1,J)+ND*G(I,J))/CN
      GO TO 694
 690  CP=CP-DO
      PTIL=(AP*P(I,J-1)+BP*P(I-1,J)+PD*G(I,J))/CP
      P(I+1,J)=DO*P(I,J)/DP
      OTIL=(AO*O(I,J-1)+BO*O(I-1,J)+DO*O(I+1,J)+ND*G(I,J))/CN
      GO TO 694
 692  CN=CN-BP
      OTIL=(AO*O(I,J-1)+DO*O(I+1,J)+ND*G(I,J))/CN
      O(I-1,J)=BP*O(    )/BO
 694  CONTINUE
      P(I,J)=(1.-OMEGA)*POLD+OMEGA*PTIL
      O(I,J)=(1.-OMEGA)*OLD+OMEGA*OTIL
      IF(P(I,J).LT.0.) P(I,J)=0.
      IF(O(I,J).LT.0.) O(I,J)=0.
      IF(O(I,J).GT.CMAX) O(I,J)=CMAX
      IF(P(I,J).GT.CMAX) P(I,J)=CMAX
 706  CONTINUE
      OMEGA=1.7
C        END OF CONCENTRATION LOOP
C   *********************************************************************
C        COMPUTE THE SPACE CHARGE AT THE FIELD POINTS.
      J=3
      DO 109 I=2,IUP
      RHO=G*(CS(J)+P(I,J)-O(I,J))
      QS(I,J)=1.E-8*ACR(I)*H*RHO +1.E-4*ACR(I)*QSS1
 109  CONTINUE
      DO 110 J=4,K3
      DO 110 I=2,IUP
      RHO=G*(CS(J)+P(I,J)-O(I,J))
      QS(I,J)=1.E-8*ACR(I)*H*RHO
 110  CONTINUE
      J=J3
      DO 111 I=2,IUP
      RHO=G*(CS(J)+P(I,J)-O(I,J))
      QS(I,J)=1.E-8*ACR(I)*H*RHO+1.E-4*ACR(I)*QSS2
 111  CONTINUE
C     RELAX THE U(I,J) FIELD THROUGH SAPP.,SIL.,AND OXIDE.
      JHI=J4-1
      DO 116 J=2,JHI
      DO 114 I=2,IUP
```

ORIGINAL PAGE IS
OF POOR QUALITY

```
      A=ACR(I)*ACZ(J)
      B=BCR(I)*BCZ(J)
      D=DCR(I)*DCZ(J)
      E=ECR(I)*ECZ(J)
      C=A+B+D+E
      UOLD=U(I,J)
      UTIL=(A*U(I,J-1)+B*U(I-1,J)+D*U(I+1,J)+E*U(I,J+1)+QS(I,J))/C
      U(I,J)=(1.-OMEGA)*UOLD+OMEGA*UTIL
      IF(U(I,J).GT.PHI(J))   U(I,J)=PHI(J)
      DU=U(I,J)-UOLD
      RES=RES+DU**2
  114 CONTINUE
  116 CONTINUE
      IF(RES.GT.1.E10) RES=1.E10
      RMS=SQRT(RES/((I7-1)*(J4-1)))
      IF(MWRIT.GT.0) WRITE(6,514) RMS
      ERRU=RMS
      RES=0.0
      ILO=I8+1
      DO 118 I=ILO,IUP
      A=ACR(I)*ACZ(J4)
      B=BCR(I)*BCZ(J4)
      D=DCR(I)*DCZ(J4)
      E=ECR(I)*ECZ(J4)
      C=A+B+D+E
      UOLD=U(I,J4)
      M=1+I-I8
      UTIL=(A*U(I,J4-1)+B*U(I-1,J4)+D*U(I+1,J4)+E*UA(M,2))/C
      U(I,J4)=(1.-OMEGA)*UOLD+OMEGA*UTIL
      UA(M,1)=U(I,J4)
      DU=U(I,J4)-UOLD
      RES=RES+DU**2
  118 CONTINUE
C     RELAX THE UA-FIELD.
      JLO=J4+1
      JHI=J5-1
      DO 122 J=JLO,JHI
      L=J-J4+1
      DO 120 I=ILO,IUP
      M=1+I-I8
      A=ACR(I)*ACZ(J)
      B=BCR(I)*BCZ(J)
      D=DCR(I)*DCZ(J)
      E=ECR(I)*ECZ(J)
      C=A+B+D+E
      UOLD=UA(M,L)
      UTIL=(A*UA(M,L-1)+B*UA(M-1,L)+D*UA(M+1,L)+E*UA(M,L+1))/C
      UA(M,L)=(1.-OMEGA)*UOLD+OMEGA*UTIL
      DU=UA(M,L)-UOLD
      RES=RES+DU**2
  120 CONTINUE
  122 CONTINUE
      IF(RES.GT.1.E10) RES=1.E10
      RMS=SQRT(RES/((J5-J4)*(I7-I8)))
      IF(MWRIT.GT.0) WRITE(6,513) RMS
  513 FORMAT(40X,F10.3)
  514 FORMAT(20X,F10.3)
  515 LOOP=LOOP+1
      IF(LOOP.LE.LTOP) GO TO 104
C     COMPUTE THE CHARGE STORED IN THE SILICON LAYER.
C        COMPUTE THE CURRENT
      JUP=J3-1
      CUR=0.
      QSIL=0.
      DO 126 J=4,JUP
      DO 124 I=2,IUP
      QSIL=QSIL+1.E-4*QS(I,J)
      CUR=CUR+G(I,J)
  124 CONTINUE
  126 CONTINUE
      CUR=1.E-4*G*CUR
      WRITE(6,516) VJ,VG,QSIL,CUR
  516 FORMAT(/,10X,'VJ=',F10.3,5X,'VG=',F10.3,5X,'QSIL=',F10.3,5X,
     *'QSIL=',E10.3)
      IF(ERRU.LT.0.004) GO TO 517
      V(I4,42)=U(17,3)
      ILO=I4+2
      DO 134 I=ILO,I5
      M=J3+2*(I-ILO)
```

ORIGINAL PAGE IS OF POOR QUALITY

```
134   V(I,J2)=U(M,3)
      GO TO 1000
517   CONTINUE
      WRITE(6,536)
536   FORMAT(/,30X,'ABBREVIATED U-FIELD'/)
      DO 540  M=1,J4,5
      J=J4-M+1
540   WRITE(6,544)  (U(I,J),I=1,I7,8)
      WRITE(6,537)
537   FORMAT(/,30X,'ABBREVIATED N-FIELD'/)
      DO 542 M=3,J3,5
      J=J3-M+1
542   WRITE(6,544)  (O(I,J),I=1,I7,8)
      WRITE(6,538)
538   FORMAT(/,30X,'ABBREVIATED P-FIELD'/)
      DO 543 M=3,J3,5
      J=J3-M+1
543   WRITE(6,544)  (P(I,J),I=1,I7,8)
544   FORMAT(12E8.2)
      IF(MWRIT.EQ.0) GO TO 136
      WRITE(6,518)
518   FORMAT(/,20X,'U(I,J) VALUES IN 6-ADJACENT FIELDS'/)
      L=0
      ILO=1
128   L=L+1
      IUP=ILO+15
      IF(L.EQ.6)  IUP=ILO+17
      DO 132 M=1,J4
      J=J4-M+1
132   WRITE(6,520)  (U(I,J),I=ILO,IUP)
520   FORMAT(18F6.1)
      ILO=IUP
      WRITE(6,522) L
522   FORMAT(//,10X,'N=',I2,//)
      IF(L.EQ.6)  GO TO 128
136   GO TO 600
      END
```

ORIGINAL PAGE IS
OF POOR QUALITY

APPENDIX C

TWO DIMENSIONAL ANALYSIS WITH DEPLETION APPROXIMATION

```
      DIMENSION W(25,11),V(41,11),U(93,56),UA(13,7),GS(93,56)
      DIMENSION AAR(26),BAR(26),DAR(26),EAR(26)
      DIMENSION AAZ(12),BAZ(12),DAZ(12),EAZ(12)
      DIMENSION ABR(42),BBR(42),DBR(42),EBR(42)
      DIMENSION ABZ(12),BBZ(12),DBZ(12),EBZ(12)
      DIMENSION ACR(94),BCR(94),DCR(94),ECR(94)
      DIMENSION ACZ(61),BCZ(61),DCZ(61),ECZ(61)
      DIMENSION X(100),CS(61),PHI(61),ZB(12),GR(61),G(93,61)
      REAL NI,NI2
      READ(16) W,V,U,UA
      REWIND 16
310   NI=1.5E10
      NI2=NI**2
      NWRIT=0
      READ(5,804) QSS1,QSS2
804   FORMAT(2E10.3)
      LWMAX=1
      LVMAX=1
      LUMAX=1
      Q=1.6E-19
      QSS1=QSS1*Q
      QSS2=QSS2*Q
      VT=0.0259
      TEL=0.8
      TOX=0.4
      TSI=0.8
      CSS=6.E15
      TAU0=2.E-6
      BETA1=3.92
      BETA2=6.32
      PI=3.1416
      EPSA=9.4*8.854E-14
      EPSB=11.7*8.854E-14
      EPSC=3.7*8.854E-14
      EPS0=8.854E-14
      I1=9
      I2=17
      I3=25
      L1=8
      L2=8
      L3=8
      K1=10
      J1=11
      W1=140.
      W2=152.
      W3=140.
      L4=8
      I4=9
      L5=32
      I5=41
      K2=10
      J2=11
      L6=32
      I6=33
      L7=92
      I7=93
      I8=82
      K3=50
      J3=51
      K4=55
      J4=56
      K5=60
      J5=61
      H=TSI/(J3-3)
C     COMPUTE COEFFICIENTS IN W-FIELD
      DO 2 I=1,I1
2     X(I)=(I-1)*W1/L1
      DO 4 I=I1,I2
4     X(I)=W1+(I-I1)*W2/L2
      DO 6 I=I2,I3
6     X(I)=W1+W2+(I-I2)*W3/L3
```

```
      I0=I3-1
      DO 8 I=2,I0
      AAR(I)=PI*(X(I+1)-X(I-1))*(X(I+1)+2.*X(I)+X(I-1))/4.
      BAR(I)=PI*(X(I)+X(I-1))/(X(I)-X(I-1))
      DAR(I)=PI*(X(I+1)+X(I))/(X(I+1)-X(I))
    8 FAR(I)=PI*X(I)*(X(I+1)-X(I))
      ALPHA=1.7
      DO 10 J=1,J1
   10 X(J)=-TSI*(ALPHA**(J1-J)-1.)/(ALPHA-1.)
      DO 12 J=2,K1
      AAZ(J)=EPSA/(X(J)-X(J-1))
      BAZ(J)=EPSA*(X(J+1)-X(J))/2.
      DAZ(J)=BAZ(J)
   12 FAZ(J)=EPSA/(X(J+1)-X(J))
C     CALCULATE COEFFICIENTS FOR V-FIELD.
      DO 14 I=1,I4
   14 X(I)=(I-1)*W1/(4.*L4)+3.*W1/4.
      DO 16 I=I4,I5
   16 X(I)=(I-I4)*W2/L5+W1
      I0=I5-1
      DO 18 I=2,I0
      ABR(I)=PI*(X(I+1)-X(I-1))*(X(I+1)+2.*X(I)+X(I-1))/4.
      BBR(I)=PI*(X(I)+X(I-1))/(X(I)-X(I-1))
      DBR(I)=PI*(X(I+1)+X(I))/(X(I+1)-X(I))
   18 FBR(I)=ABR(I)
      KA=J3-3
      ALPHA=1.25
   20 AN=(ALPHA**K2-1.-KA*(ALPHA-1.))*(ALPHA-1.)
      AD=(K2-1)*ALPHA**K2-K2*ALPHA**(K2-1)+1.
      DA=-AN/AD
      ALPHA=ALPHA+DA
      RATIO=ABS(DA/ALPHA)
      IF(RATIO.GT.0.01) GO TO 20
      HO=TSI/(J3-3)
      DO 22 J=1,J2
   22 ZB(J)=-HO*(ALPHA**(J2-J)-1.)/(ALPHA-1.)
      DO 24 J=2,K2
      ABZ(J)=EPSA/(ZB(J)-ZB(J-1))
      BBZ(J)=EPSA*(ZB(J+1)-ZB(J-1))/2.
      DBZ(J)=BBZ(J)
   24 FBZ(J)=EPSA/(ZB(J+1)-ZB(J))
C     COEFFICIENTS FOR U-FIELD.
      DO 26 I=1,I6
   26 X(I)=(I-1)*W2/(2.*L2*L6)+W1
      DO 28 I=I6,I7
   28 X(I)=X(I6)+(I-I6)*W2/(2.*L5)
      I0=I7-1
      DO 30 I=2,I0
      ACR(I)=PI*(X(I+1)-X(I-1))*(X(I+1)+2.*X(I)+X(I-1))/4.
      BCR(I)=PI*(X(I)+X(I-1))/(X(I)-X(I-1))
      DCR(I)=PI*(X(I+1)+X(I))/(X(I+1)-X(I))
   30 FCR(I)=ACR(I)
      X(1)=ZB(J2-2)
      X(2)=ZB(J2-1)
      X(3)=0.
      DO 32 J=4,J3
   32 X(J)=TSI*(J-3)/(J3-3)
      DO 34 J=J3,J4
   34 X(J)=X(J3)+TOX*(J-J3)/(J4-J3)
      DO 36 J=J4,J5
   36 X(J)=X(J4)+TEL*(J-J4)/(J5-J4)
      ACZ(2)=EPSA/(X(2)-X(1))
      BCZ(2)=EPSA*(X(3)-X(1))/2.
      DCZ(2)=BCZ(2)
      FCZ(2)=EPSA/(X(3)-X(2))
      ACZ(3)=EPSA/(X(3)-X(2))
      BCZ(3)=(EPSB*(X(4)-X(3))+EPSA*(X(3)-X(2)))/2.
      DCZ(3)=BCZ(3)
      FCZ(3)=EPSB/(X(4)-X(3))
      DO 38 J=4,K3
      ACZ(J)=EPSB/(X(J)-X(J-1))
      BCZ(J)=EPSB*(X(J+1)-X(J-1))/2.
      DCZ(J)=BCZ(J)
   38 FCZ(J)=EPSB/(X(J+1)-X(J))
      ACZ(J3)=EPSB/(X(J3)-X(J3-1))
      BCZ(J3)=(EPSC*(X(J3+1)-X(J3))+EPSB*(X(J3)-X(J3-1)))/2.
      DCZ(J3)=BCZ(J3)
      FCZ(J3)=EPSC/(X(J3+1)-X(J3))
      J0=J4-1
```

```
      JL=J3+1
C     DO THE OXIDE REGION.
      DO 40 J=JL,JU
      ACZ(J)=EPSC/(X(J)-X(J-1))
      BCZ(J)=EPSC*(X(J+1)-X(J))/2.
      BCZ(J)=BCZ(J)
   40 CCZ(J)=EPSC/(X(J+1)-X(J))
      ACZ(J4)=EPSC/(X(J4)-X(J4-1))
      BCZ(J4)=(EPSO*(X(J4+1)-X(J4))+EPSC*(X(J4)-X(J4-1)))/2.
      BCZ(J4)=BCZ(J4)
      CCZ(J4)=EPSO/(X(J4+1)-X(J4))
      JL=J4+1
      JU=J5-1
      DO 42 J=JL,JU
      ACZ(J)=EPSO/(X(J)-X(4-1))
      BCZ(J)=EPSO*(X(J+1)-X(J))/2.
      BCZ(J)=BCZ(J)
   42 CCZ(J)=EPSO/(X(J+1)-X(J))
C     COMPUTE DOPING AND LIFETIME DISTRIBUTIONS.
      DO 43 J=3,J3
      CS(J)=CSS*EXP(-BETA1*(TSI-X(J)))
      PHI(J)=VT*BETA1*X(J)
   43 TN(J)=0.5*NI*EXP(BETA2*(TSI-X(J)))/TAUO
  800 READ(5,802) VJ,VG,ITERM,LWRIT
  802 FORMAT(2F10.3,2I10)
      IF(VG.GT.0.0) GO TO 810
      VG=VG-1.1
      VINV=VG-2.*VT*ALOG(CS(J3)/NI)
C     SET ALL FIXED BOUNDARY VALUES.
      DO 44 I=1,I1
   44 V(I,J1)=VG
      DO 45 I=1,I8
   45 W(I,J2)=VG
      DO 46 I=I2,I3
   46 V(I,J1)=0.
      DO 48 J=3,J3
      W(1,J)=VJ
   48 W(I7,J)=PHI(J)
      DO 50 J=J3,J4
      W(1,J)=VJ+(J-J3)*(VG-VJ)/(J4-J3)
   50 W(I7,J)=PHI(J3)
      DO 52 I=1,I8
   52 W(I,J4)=VG
      IU=1+I7-I8
      DO 54 J=1,6
      WA(1,J)=VG
   54 WA(IU,J)=PHI(J3)
      DO 56 I=1,I8
   56 WA(I,6)=VG-(I-1)*(VG-PHI(J3))/(I7-I8)
C     START IN W-FIELD WITH RELAXATION.
      IPASS=0
      INCR=1
 1000 CONTINUE
      IPASS=IPASS+1
      MWRIT=0
      IF(IPASS/INCR.EQ.LWRIT) MWRIT=1
ERROR*  THIS STATEMENT CONTAINS IMPLIED MULTIPLICATION.
      ICON=(-1)**(IPASS)                    3 ——— Delete the 3
      IU=I2-1
      IA=I1+1
      DO 62 I=IA,I8
      IP=4+I-3*I1
   62 W(I,J1)=V(IP,J2)
      OMEGA=1.8
      RID=0.
      LOOP=1
      IOP=I3-1
      JLO=J1-1
      JHI=2
      JJ=-1
      IF(ICON.EQ.-1) GO TO 64
      JLO=2
      JHI=J1-1
      JJ=1
   64 CONTINUE
      RES=0.
      DO 68 J=JLO,JHI,JJ
      DO 66 I=2,IOP
      OLD=W(I,J)
```

```
      A=AAR(I)*AAZ(J)
      B=BAR(I)*BAZ(J)
      D=DAR(I)*DAZ(J)
      F=EAR(I)*EAZ(J)
      C=A+B+D+E
      WTIL=(A*W(I,J-1)+B*W(I-1,J)+D*W(I+1,J)+F*W(I,J+1))/C
      W(I,J)=(1.-OMEGA)*WOLD+OMEGA*WTIL
      DW=W(I,J)-WOLD
      RES=RES+DW**2
   66 CONTINUE
      W(1,J)=W(2,J)
      W(I3,J)=W(IUP,J)
   68 CONTINUE
      DO 70 I=1,I3
      W(I,1)=W(I,2)
   70 CONTINUE
      LOOP=LOOP+1
      IF(LOOP.LE.LWMAX) GO TO 64
      IF(WRIT.EQ.0) GO TO 77
      RMS=SQRT(RES)
      WRITE(6,500)
  500 FORMAT(/,20X,'DATA FOR W(I,J) FIELD',/)
      WRITE(6,502) RMS
  502 FORMAT(/,20X,'RMS=',F6.3,/)
      DO 72 M=1,J1
      J=J1+1-M
      WRITE(6,506) (W(I,J),I=1,I3,2)
   72 CONTINUE
  506 FORMAT(10X,13F8.2)
   77 CONTINUE
C     DO THE V-FIELD.
C     LOCATE BOUNDARY VALUES IN W AND U FIELDS AND INTERPOLATE.
      IW=1+3*I1/4
      IR=I2-1
      DO 78 I=IW,IR
      VLO=W(I,K1)
      VHI=W(I+1,K1)
      K=4*(I-IW)+1
      V(K,1)=VLO
      V(K+1,1)=VLO+(VHI-VLO)/4.
      V(K+2,1)=VLO+(VHI-VLO)/2.
      V(K+3,1)=VLO+3.*(VHI-VLO)/4.
      V(K+4,1)=VHI
   78 CONTINUE
      DO 82 J=2,J2
      S=(ZB(J)-ZB(1))/ZB(1)
      V(1,J)=W(I1,K1)-S*(W(I1,J1)-W(I1,K1))
      V(I5,J)=W(I2,K1)-S*(W(I2,J1)-W(I2,K1))
   82 CONTINUE
      IF(IPASS.GT.1) GO TO 85
      V(I4+1,J2)=U(17,3)
      ILO=I4+2
      DO 84 I=ILO,I5
      M=33+2*(I-ILO)
      V(I,J2)=U(M,3)
   84 CONTINUE
   85 CONTINUE
C     RELAX THE V-FIELD.
      OMEGA=1.8
      LOOP=1
      IUP=I5-1
      JLO=J2-1
      JHI=2
      JJ=-1
      IF(ICON.EQ.-1) GO TO 86
      JLO=2
      JHI=J2-1
      JJ=1
   86 CONTINUE
      RES=0.
      DO 90 J=JLO,JHI,JJ
      DO 88 I=2,IUP
      A=ABR(I)*ABZ(J)
      B=BBR(I)*BBZ(J)
      D=DBR(I)*DBZ(J)
      F=EBR(I)*EBZ(J)
      C=A+B+D+F
      WOLD=V(I,J)
      VTIL=(A*V(I,J-1)+B*V(I-1,J)+D*V(I+1,J)+F*V(I,J+1))/C
```

```
      V(I,J)=(1.-OMEGA)*VOLD+OMEGA*VTIL
      DV=V(I,J)-VOLD
      RES=RES+DV**2
   68 CONTINUE
   60 CONTINUE
      LOOP=LOOP+1
      IF(LOOP.LE.LVMAX) GO TO 96
      IF(MWRIT.EQ.0) GO TO 95
      WRITE(6,508)
  508 FORMAT(/,20X,'DATA FOR V(I,J) FIELD',/)
      WRITE(6,502) RMS
      DO 92 M=1,J2
      J=J2-M+1
      WRITE(6,510) (V(I,J),I=1,I5,4)
   92 CONTINUE
  510 FORMAT(10X,11F8.2)
   95 CONTINUE
C     DO THE RELAXATION FOR THE U-FIELD
C     LOAD BOUNDARY VALUES FROM THE V-FIELD AND INTERPOLATE.
      U(1,1)=V(14,J2-2)
      U(1,2)=V(14,J2-1)
      U(I7,1)=V(I5,J2-2)
      U(I7,2)=V(I5,J2-1)
      U(17,1)=V(I4+1,J2-2)
      DO96  I=I6,I7,2
      M=I4+2+(I-I6)/2
      U(I,1)=V(M,J1-2)
   96 CONTINUE
      DO 98 I=2,16
      U(I,1)=U(1,1)+(I-1)*(U(17,1)-U(1,1))/16
   98 CONTINUE
      DO 100 I=18,32
      U(I,1)=U(17,1)+(I-17)*(U(33,1)-U(17,1))/16
  100 CONTINUE
      IUP=I7-1
      DO 102 I=34,IUP,2
      U(I,1)=(U(I-1,1)+U(I+1,1))/2.
  102 CONTINUE
      RES=0.0
      LOOP=1
      OMEGA=1.8
  104 CONTINUE
C ***********************************************************************
C           COMPUTE SPACE CHARGE AND GENERATION RATE.
      J=3
      DO 702 I=2,IUP
      RHO=0.
      GEN=0.
      UTEST=0.0
      IF(U(I,J).GE.UTEST) GO TO 700
      RHO=Q*CS(J)
      GEN=GR(J)
  700 DVOL=1.E-6*ACR(I)*H/2.
      S(I,J)=DVOL*RHO+1.E-4*ACR(I)*QSS1
      G(I,J)=DVOL*GEN
  702 CONTINUE
      DO 706 J=4,K3
      DO 706 I=2,IUP
      RHO=0.
      GEN=0.
      UTEST=0.0
      IF(U(I,J).GE.UTEST) GO TO 704
      RHO=Q*CS(J)
      GEN=GR(J)
  704 DVOL=1.E-6*ACR(I)*H
      S(I,J)=DVOL*RHO
      G(I,J)=DVOL*GEN
  706 CONTINUE
      J=J3
      DO 710 I=2,IUP
      RHO=0.
      GEN=0.
      UTEST=0.0
      IF(U(I,J).GE.UTEST) GO TO 708
      RHO=Q*CS(J)
      GEN=GR(J)
  708 DVOL=1.E-6*ACR(I)*H/2.
      S(I,J)=DVOL*RHO+1.E-4*ACR(I)*QSS2
      G(I,J)=DVOL*GEN
```

```
  710 CONTINUE
C     RELAX THE U(I,J) FIELD THROUGH SAPP.,SIL.,AND OXIDE.
      DUMAX=0.
      JLO=J4-1
      JHI=2
      JJ=-1
      IF(ICON.EQ.-1) GO TO 105
      JLO=2
      JHI=J4-1
      JJ=1
  105 DO 116 J=JLO,JHI,JJ
      DO 114 I=2,IUP
      A=ACR(I)*ACZ(J)
      B=BCR(I)*BCZ(J)
      D=DCR(I)*DCZ(J)
      E=ECR(I)*ECZ(J)
      C=A+B+D+E
      UOLD=U(I,J)
      UTIL=(A*U(I,J-1)+B*U(I-1,J)+D*U(I+1,J)+E*U(I,J+1)+QS(I,J))/C
      U(I,J)=(1.-OMEGA)*UOLD+OMEGA*UTIL
      IF(U(I,J).GT.PHI(J))  U(I,J)=PHI(J)
      IF(J.EQ.J3) GO TO 109
      GO TO 110
  109 IF(U(I,J).LT.VINV) U(I,J)=VINV
  110 ABDU=ABS(U(I,J)-UOLD)
      IF(ABDU.GT.DUMAX) DUMAX=ABDU
  114 CONTINUE
  116 CONTINUE
      IF(MARIT.GT.0) WRITE(6,514) DUMAX
      ILO=I8+1
      DO 118 I=ILO,IUP
      A=ACR(I)*ACZ(J4)
      B=BCR(I)*BCZ(J4)
      D=DCR(I)*DCZ(J4)
      E=ECR(I)*ECZ(J4)
      C=A+B+D+E
      UOLD=U(I,J4)
      M=1+I-I8
      UTIL=(A*U(I,J4-1)+B*U(I-1,J4)+D*U(I+1,J4)+E*UA(M,2))/C
      U(I,J4)=(1.-OMEGA)*UOLD+OMEGA*UTIL
      UA(M,1)=U(I,J4)
      ABDU=ABS(U(I,J4)-UOLD)
      IF(ABDU.GT.DUMAX) DUMAX=ABDU
  118 CONTINUE
C     RELAX THE UA-FIELD.
      JLO=J4+1
      JHI=J5-1
      DO 122 J=JLO,JHI
      L=J-J4+1
      DO 120 I=ILO,IUP
      M=1+I-I8
      A=ACR(I)*ACZ(J)
      B=BCR(I)*BCZ(J)
      D=DCR(I)*DCZ(J)
      E=ECR(I)*ECZ(J)
      C=A+B+D+E
      UOLD=UA(M,L)
      UTIL=(A*UA(M,L-1)+B*UA(M-1,L)+D*UA(M+1,L)+E*UA(M,L+1))/C
      UA(M,L)=(1.-OMEGA)*UOLD+OMEGA*UTIL
      ABDU=ABS(UA(M,L)-UOLD)
      IF(ABDU.GT.DUMAX) DUMAX=ABDU
  120 CONTINUE
  122 CONTINUE
      IF(MARIT.GT.0) WRITE(6,513) DUMAX
  513 FORMAT(40X,F10.3)
  514 FORMAT(20X,F10.3)
  515 LOOP=LOOP+1
      IF(LOOP.LE.LUMAX) GO TO 104
      IF(MARIT.GT.0) GO TO 517
      U(I4+1,J2)=U(17,3)
      ILO=I4+2
      DO 134 I=ILO,I5
      M=J3+2*(I-ILO)
  134 U(I,J2)=U(M,3)
      GO TO 1000
  517 CONTINUE
C     COMPUTE THE CHARGE STORED IN THE SILICON LAYER.
C        COMPUTE THE CURRENT
      IUP=J3-1
```

```
      CUR=0.
      QSIL=0.
      QEL=0.
      DO 126 J=4,JUP
      DO 124 I=2,IUP
      QSIL=QSIL+1.E-4*QS(I,J)
      CUR=CUR+G(I,J)
124   CONTINUE
126   CONTINUE
      DO 125 I=2,IUP
      QEL=QEL+ACR(I)*(U(I,J4)-U(I,K4))
125   CONTINUE
      QEL=1.E-4*EPSC*QEL*(J4-J3)/TOX
      CUR=1.E-4*Q*CUR
      WRITE(6,516) VJ,VG,QSIL,QEL,CUR
516   FORMAT(/,10X,'VJ=',F10.3,5X,'VG=',F10.3,5X,'QSIL=',F10.5,5X,
     *'QEL=',F11.5,5X,'ISIL=',E10.5)
      WRITE(6,536)
536   FORMAT(/,30X,'ABBREVIATED U-FIELD'/)
      DO 540  M=1,J4,5
      J=J4-M+1
540   WRITE(6,544) (U(I,J),I=1,I7,8)
      WRITE(6,537)
537   FORMAT(/,30X,'ABBREVIATED QS-FIELD'/)
      DO 542 M=3,J3,4
      J=J3-M+3
542   WRITE(6,544) (QS(I,J),I=1,I7,8)
      WRITE(6,538)
538   FORMAT(/,30X,'ABBREVIATED G-FIELD'/)
      DO 543 M=3,J3,4
      J=J3-M+3
543   WRITE(6,544) (G(I,J),I=1,I7,8)
544   FORMAT(12E10.2)
      WRITE(6,546) IPASS
546   FORMAT(/,20X,'IPASS=',I4/)
      INCR=INCR+1
      IF(IPASS.EQ.ITERM) GO TO 800
      GO TO 1000
810   CONTINUE
      WRITE(16) W,V,U,UA
      REWIND 16
      STOP
      END
```

ORIGINAL PAGE IS
OF POOR QUALITY

☆ U.S. GOVERNMENT PRINTING OFFICE 1978-641-255/393 REGION NO. 4